J Dyn Diff Equat (2016) 28:1215–1263
DOI 10.1007/s10884-015-9484-4

Periodic Solutions of a Singularly Perturbed Delay Differential Equation with Two State-Dependent Delays

A. R. Humphries[1] · D. A. Bernucci[1,2] · R. C. Calleja[3] · N. Homayounfar[1,4] · M. Snarski[1,5]

Received: 21 November 2014 / Revised: 21 August 2015 / Published online: 28 December 2015

Abstract Periodic orbits and associated bifurcations of singularly perturbed state-dependent delay differential equations (DDEs) are studied when the profiles of the periodic orbits contain jump discontinuities in the singular limit. A definition of singular solution is introduced which is based on a continuous parametrisation of the possibly discontinuous limiting solution. This reduces the construction of the limiting profiles to an algebraic problem. A model two state-dependent DDE is studied in detail and periodic singular solutions are constructed with one and two local maxima per period. A complete characterisation of the conditions on the parameters for these singular solutions to exist facilitates an investigation of bifurcation structures in the singular case revealing folds and possible cusp bifurcations. Sophisticated boundary value techniques are used to numerically compute the bifurcation diagram of the state-dependent DDE when the perturbation parameter is close to zero. This confirms that the solutions and bifurcations constructed in the singular case persist when the perturbation

✉ A. R. Humphries
tony.humphries@mcgill.ca

D. A. Bernucci
dbernucci3@math.gatech.edu

R. C. Calleja
calleja@mym.iimas.unam.mx

N. Homayounfar
namdar.homayounfar@mail.utoronto.ca

M. Snarski
Michael_Snarski@Brown.edu

1 Department of Mathematics and Statistics, McGill University, Montreal, QC H3A 0B9, Canada

2 Present Address: School of Mathematics, Georgia Institute of Technology, Atlanta, GA 30332-0160, USA

3 Depto. Matemáticas y Mecánica, IIMAS, Universidad Nacional Autónoma de México, 01000 Mexico, Mexico

4 Present Address: Department of Statistics, University of Toronto, Toronto, ON M5S 3G3, Canada

5 Present Address: Division of Applied Mathematics, Brown University, Providence, RI 02912, USA

parameter is nonzero, and hence demonstrates that the solutions constructed using our singular solution definition are useful and relevant to the singularly perturbed problem. Fold and cusp bifurcations are found very close to the parameter values predicted by the singular solution theory, and we also find period-doubling bifurcations as well as periodic orbits with more than two local maxima per period, and explain the alignment between the folds on different bifurcation branches.

Keywords State-dependent delay differential equations · Bifurcation theory · Periodic solutions · Singularly perturbed solutions · Numerical approximation

Mathematics Subject Classification 34K18 · 34K13 · 34K26 · 34K28

1 Introduction

We consider periodic solutions of the singularly perturbed scalar state-dependent delay differential equation (DDE)

$$\varepsilon\dot{u}(t) = -u(t) - K_1 u(t - a_1 - cu(t)) - K_2 u(t - a_2 - cu(t)), \tag{1.1}$$

which has two linearly state-dependent delays, and no other nonlinearity apart from the state-dependency of the delays. We consider $\varepsilon \geqslant 0$, $c > 0$, $a_i > 0$, $K_i > 0$, and without loss of generality we order the terms so that $a_2 > a_1 > 0$. Equation (1.1) is an example of a singularly perturbed scalar DDE with N state-dependent delays of the form

$$\varepsilon\dot{u}(t) = f(t, u(t), u(\alpha_1(t, u(t))), \ldots, u(\alpha_N(t, u(t)))), \quad u(t) \in \mathbb{R}. \tag{1.2}$$

We will define a concept of singular solution for (1.2) based on a continuous parametrisation. This essentially entails defining a singular limit for Eq. (1.2), resulting in an equation whose solutions can in principle be found algebraically. In the case of (1.1) we construct several such classes of singular periodic solutions, and investigate the codimension-one and -two bifurcations that occur.

DDEs arise in many applications including engineering, economics, life sciences and physics [12,24,37]. There is a well established theory for functional differential equations as infinite-dimensional dynamical systems [9,16], which encompasses DDEs with constant or prescribed delay. However, many problems that arise in applications have delays which depend on the state of the system (see for example [13,20,23,38]). Such state-dependent DDEs fall outside of the scope of the previously developed theory and have been the subject of much study in recent years. See [17] for a relatively recent review of the general theory of state-dependent DDEs.

The study of singularly perturbed DDEs already stretches over several decades. As early as 1985 Magalhaẽs [25] recognised that singularly perturbed discrete DDEs have different asymptotics to singularly perturbed distributed DDEs. For equations with a single constant delay, in the singular limit the DDE reduces to a map (see (1.7) below) which describes the asymptotic behaviour when the limiting profiles are functions [21,26,35].

One of the main difficulties studying (1.2) in the singular limit is that while the solution $u(t)$ is a graph for any $\varepsilon > 0$, this need not be so in the limit as $\varepsilon \to 0$, when derivatives can become unbounded, and the resulting limiting solution can have jump discontinuities. Techniques for studying singularly perturbed DDEs with a single constant discrete delay can be found in [6,26]. In [26] slowly oscillating periodic solutions (SOPS) are proved to

converge to a square wave in the singular limit, using layer equations to describe the solution in the transition layer. In [6] for monotone nonlinearities a homotopy method is used to show that the layer equations have a unique homoclinic orbit. Mallet-Paret and Nussbaum, in a series of papers [27,29,30] extend the study of SOPS to DDEs with a single state-dependent delay. In [27] SOPS are shown to exist for all ε sufficiently small. These solutions are shown to have non-vanishing amplitude in the singular limit in [29], and under mild assumptions the discontinuity set of the limiting profile is shown to consist of isolated points. In [30] Max-plus operators are introduced to study the shape of the limiting profiles. The DDE

$$\varepsilon \dot{u}(t) = -u(t) - Ku(t - a_1 - u(t)), \tag{1.3}$$

is considered as an example in [30]. This corresponds to (1.1) with $K_2 = 0$ and $c = 1$. It is shown in [30] that the limiting profile is the "sawtooth" shown in Fig. 1b below. In [31] the SOPS of (1.3) are studied in detail and the shape of the solution near the local maxima and minima is determined for $0 < \varepsilon \ll 1$ as well as the width of the transition layer, and the "super-stability" of the solution. Other work on singularly perturbed state-dependent DDEs includes [14] where they arise from the regularisation of neutral state-dependent DDEs, and also [34] where the metastability of solutions of a singularly perturbed state-dependent DDE is studied in the case where the state-dependency vanishes in the limit as $\varepsilon \to 0$.

The studies mentioned above all considered singularly perturbed DDEs with only one delay, and either considered single solutions or a sequence of solutions as $\varepsilon \to 0$. We will study the bifurcation diagram for the two-delay DDE (1.3) when $0 \leqslant \varepsilon \ll 1$, regarding K_1 as a bifurcation parameter. Beyond those mentioned previously, the only other work we know of that tackles singularly perturbed bifurcations in state-dependent DDEs is [22], where the solutions of (1.3) with $a_1 = c = 1$ are studied close to the singular Hopf bifurcation. On the other hand, singularly perturbed ODEs frequently arise through mixed mode oscillations on multiple time-scales and their bifurcation analysis is well understood (see [8] for a review). Codimension-two bifurcations have also been studied in singularly perturbed ODEs [3,5].

The development of bifurcation theory for state-dependent DDEs has been difficult because the centre manifolds have not been shown to have the necessary smoothness [17], and a rigorous Hopf bifurcation theorem for state-dependent DDEs was first proved only in the last decade [10] (see also [15,18,36]). The numerical analysis of state-dependent DDEs is more advanced with numerical techniques for solving both initial value problems [1,2] and for computing bifurcation diagrams [11]. DDEBiftool [11] is a very useful tool for computing Hopf bifurcations and continuation of solution branches in state-dependent DDEs, and it has been used to study the bifurcations that arise in (1.1) when $\varepsilon = 1$ [4,19]. John Mallet-Paret has presented numerical simulations of (1.1) in seminars, but the only other published work of which we are aware that encompasses (1.1) is [28]. There the existence of SOPs was proved for (1.2) with suitable nonlinearities when $\alpha_i(t, u(t)) = t - \tau_i(u(t))$ with $\tau_i(0) = k \neq 0$ for all i. Mallet-Paret and Nussbaum have announced results for the existence of periodic orbits in state-dependent DDEs with two delays including equations of the form (1.1), but these results are as yet unpublished [32].

In [19] a largely numerical investigation of (1.1) with $\varepsilon = \mathcal{O}(1)$ revealed fold bifurcations on the branches of periodic orbits, resulting in parameter regions with bistability of periodic orbits. While the stable periodic orbits usually had one local maxima per period, the unstable periodic orbits in the these windows of bistability often had more than one local maxima per period. In the current work we will investigate these fold bifurcations and the profiles of the periodic orbits in the singular limit $\varepsilon \to 0$.

To study (1.2) in the singular limit $\varepsilon = 0$ when the limiting profile may have jump discontinuities, we propose nested continuous parameterisations of the limiting singular

solution. We will not restrict our attention to slowly oscillating periodic orbits, but will consider both long and short period orbits. We will study the case of the two delay state-dependent DDE (1.1) in detail, and construct branches of singular periodic orbits with fold and cusp bifurcations. We will then use the predictions of this theory to guide a numerical study which will reveal branches of periodic orbits for $0 < \varepsilon \ll 1$ with profiles close to the singular limiting profiles and fold and cusp bifurcations close to the predicted parameter values. We will also find period-doubling bifurcations in the singularly perturbed problem.

Since our parametrisation technique is our main theoretical tool and crucial to all our results, we will describe it here in detail. For the outer parametrisation we consider the solution profile as a parametric curve, $\Gamma(\mu) = (t(\mu), u(\mu))$. This is a familiar concept from physics, where trajectories in space-time are parameterised, and has been used in the study of the DDEs arising from Wheeler–Feynman Electrodynamics [7]. However, in the current work we use the parametric curve $\Gamma(\mu)$ to enable us to consider continuous objects even in the singular limit. For any $\varepsilon > 0$ an injective parametrisation of the solution must have $t(\mu)$ strictly monotonic, but limiting profiles as $\varepsilon \to 0$ may have $t(\mu)$ merely monotonic. This leads us to the parametric definition of an admissible singular solution profile in Definition 1.1. In Definition 1.2 we will introduce the inner parametrisation that allows us to define singular solutions of (1.2).

Definition 1.1 Let $\Gamma : I \to \mathbb{R}^2$ be a continuous injective parametric curve defined on a nonempty interval $I \subseteq \mathbb{R}$. For $\mu \in I$ let $\Gamma(\mu) = (t(\mu), u(\mu))$. Then if $t : I \to \mathbb{R}$ is monotonically increasing we say that $\Gamma(I)$ is an *admissible singular solution profile* for (1.2).

Although $t(\mu)$ is not required to be a strictly monotonically increasing function to be an admissible singular solution profile, it is important to note that on any subinterval I_i on which $t(\mu)$ is constant, the injectivity requirement ensures that $u(\mu)$ is strictly monotonic. Thus we partition the interval I as $I = I^+ \cup I^- \cup I^*$ where

1. I^* a disjoint union of open intervals and $t(\mu)$ is strictly monotonically increasing on each interval,
2. $I^\pm$ are each disjoint unions of closed intervals with $t(\mu)$ constant on each such interval, and $u(\mu)$ strictly monotonically decreasing (respectively increasing) on each interval of I^- (resp. I^+).

The partition of I generates a corresponding partition of $\Gamma(I)$ as $\Gamma(I) = \Gamma^+ \cup \Gamma^- \cup \Gamma^*$. For (1.1) we will find that $I^+ = \emptyset$, and so I^* and I^- will both be unions of disjoint intervals which we may write as

$$I^* = \bigcup_i I_{2i} = \bigcup_i (b_{2i}, b_{2i+1}), \quad I^- = \bigcup_i I_{2i+1} = \bigcup_i [b_{2i+1}, b_{2i+2}],$$

for a sequence of strictly increasing real numbers b_i. See Fig. 1 for an example.

The partition of $\Gamma(I)$ as $\Gamma(I) = \Gamma^+ \cup \Gamma^- \cup \Gamma^*$ is similar that of $\Omega = \Omega^+ \cup \Omega^- \cup \Omega^*$ introduced by Mallet-Paret and Nussbaum [29] (see also Sect. 4 of [30]). In their work Ω is defined as the limiting set for a sequence of solutions as $\varepsilon \to 0$, while $\Omega^\pm$ are defined as the sets of points for which $\liminf \pm\varepsilon\dot{u}(t) > 0$, which results in $\Omega^\pm$ being relatively open subsets of Ω. In contrast, we define $\Gamma(I)$ and its partition directly from the parametrisation of the admissible singular solution profile, with $\Gamma^\pm$ being closed subsets of Ω. Now intuitively, since Γ^* defines the parts of the singular solution profile for which $\dot{u}$ is finite, from (1.2) it should correspond to the parts of the solution for which $\lim_{\varepsilon\to 0} f(t, u(t), u(\alpha_1(t, u(t))), \ldots, u(\alpha_N(t, u(t)))) = 0$. Similarly $\dot{u} = \pm\infty$ on $\Gamma^\pm$

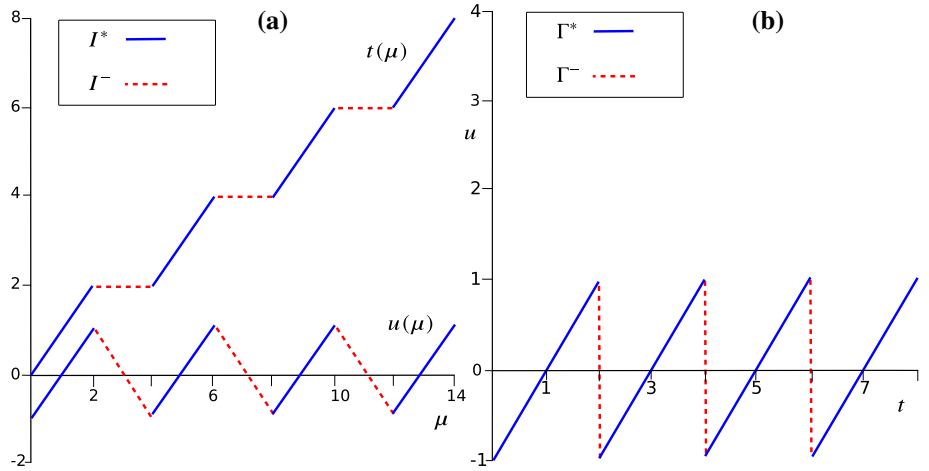

Fig. 1 An admissible singular solution. **a** The functions $t(\mu)$ and $u(\mu)$ for $\mu \in I = [0, 14]$. **b** The corresponding admissible singular solution profile $\Gamma(I) = \Gamma^* \cup \Gamma^- \in \mathbb{R}^2$

should imply that $\lim_{\varepsilon \to 0} f(t, u(t), u(\alpha_1(t, u(t))), \ldots, u(\alpha_N(t, u(t))))$ is respectively positive or negative. Rather than treating this process as $\varepsilon \to 0$ we introduce an extra level of parametrisation, so that we can write the right-hand side of (1.2) as a function of a single parametrisation variable, which allows us to treat the $\varepsilon = 0$ case directly in a continuous framework.

Definition 1.2 Let Γ be an admissible singular solution profile defined on $I \subseteq \mathbb{R}$ and let $J \subseteq \mathbb{R}$ be a nonempty interval. Let $\mu_i : J \to I$ for $i = 0, \ldots, N$ be continuous functions with $\mu_0(\eta)$ monotonically increasing. Define $J^* = \text{cl}\{\eta : \mu_0(\eta) \in I^*\}$ and $J^{\pm} = \text{int}\{\eta : \mu_0(\eta) \in I^{\pm}\}$, and let

$$F(\eta) = f(t(\mu_0(\eta)), u(\mu_0(\eta)), u(\mu_1(\eta)), \ldots, u(\mu_N(\eta))). \tag{1.4}$$

Then if

$$t(\mu_i(\eta)) = \alpha_i(t(\mu_0(\eta)), u(\mu_0(\eta))), \quad \forall \eta \in J, \ \forall i = 1, \ldots, N, \tag{1.5}$$

and

1. $F(\eta) = 0$ for all $\eta \in J^*$,
2. $F(\eta) < 0$ for all $\eta \in J^-$,
3. $F(\eta) > 0$ for all $\eta \in J^+$.

we say that $\{\Gamma, \mu_0, \ldots, \mu_N\}$ define a *singular solution* for (1.2) on the interval $t(\mu_0(J))$.

In the definition, essentially one can think of $t(\mu_0(\eta))$ as the current time, and $t(\mu_i(\eta))$ as the delayed times. Then (1.5) simply says that the delayed times are given by the formula for α_i from the DDE (1.2), while (1.4) reduces the right-hand side of (1.2) to a continuous function of the inner parametrisation variable. Any solution of (1.2) for $\varepsilon > 0$ can be similarly parameterised, resulting in

$$\varepsilon \dot{u}(t(\mu_0(\eta))) = F(\eta). \tag{1.6}$$

Now the conditions on $F(\eta)$ in the definition for a singular solution with $\varepsilon = 0$ follow from the remarks on the sets Γ^*, $\Gamma^{\pm}$ before the definition.

This concept of singular solution generalises that of [21,26,35]. To see this, consider the case where Eq. (1.2) is autonomous with one fixed delay, so $N = 1$ and $\alpha_1(t, u(t)) = t - \tau$ for some constant $\tau > 0$. Suppose also that the limiting profile is a graph, so $\Gamma^- = \Gamma^+ = \emptyset$. Then we can define a singular solution following Definition 1.2 with $\mu_0(\eta) = \eta$, $\mu_1(\eta) = \eta - \tau$, and $t = t(\mu) = \mu$. This parametrisation respects (1.5), and since $\Gamma^- = \Gamma^+ = \emptyset$ we have $J^* = J$ and require $F(\eta) = 0$ for all $\eta \in J$. But then

$$0 = F(\eta) = f(u(\mu_0(\eta)), u(\mu_1(\eta))) = f(u(\eta), u(\eta - \tau)) = f(u(t), u(t - \tau)),$$

and we are left to consider

$$f(u(t), u(t - \tau)) = 0, \tag{1.7}$$

which is the equation studied in [21,26,35]. Thus in the case that $\Gamma^- = \Gamma^+ = \emptyset$ our definition encompasses that of [21,26,35]. However, in this work we will be interested in the case where Γ^- is not empty, and the delays are not constant.

If $J = \mathbb{R}$ and there exists $T > 0$ and $\eta_T > 0$ such that

$$t(\mu_i(\eta + \eta_T)) = t(\mu_i(\eta)) + T, \quad u(\mu_i(\eta + \eta_T)) = u(\mu_i(\eta)), \quad \forall i = 1, \ldots, N, \quad \forall \eta \in \mathbb{R},$$

we say that the singular solution is periodic. The period is the smallest such $T > 0$.

The main aim of this paper is to initiate a study of periodic solutions of the singularly perturbed two-delay DDE (1.1). We will construct singular periodic solutions (as per Definition 1.2), and will find both unimodal sawtooth solutions that correspond to the profile seen in Fig. 1 and bimodal solutions which have two "teeth" per period. The labels *unimodal* and *bimodal* are used throughout to indicate the number of local maxima of the solution per period. Although superficially the unimodal solutions look similar to those found in the one delay case, the interaction between the two state-dependent delays adds both complications to the derivations and richness to the dynamics observed. We will demonstrate numerically using DDEBiftool [11], a sophisticated numerical bifurcation package for DDEs, that the singular solutions and associated bifurcation structures that we find persist for $\varepsilon > 0$.

In Sect. 2 as an example we first consider (1.3) with one delay, for which Mallet-Paret and Nussbaum [30,31] have already established the so-called *sawtooth* limiting profile, as illustrated in Fig. 1b. We construct the corresponding singular solution following Definition 1.2. We then consider the two-delay problem (1.1) and in Theorem 2.2 establish conditions on the parameters for this to have a sawtooth solution. In (2.16) and (2.17) we introduce two admissible singular solution profiles which have two local maxima per period. Theorems 2.3 and 2.4 present singular solutions for these profiles and establish the constraints on the parameters for them to exist. Since these solutions have two local maxima per period, we refer to them as type I and type II bimodal (periodic) solutions.

In Sect. 3 we treat K_1 as a bifurcation parameter and in Theorems 3.1, 3.3 and 3.4 identify intervals of the parameter K_1 for which unimodal, type I bimodal and type II bimodal solutions exist. We will also find singular fold bifurcations in Theorem 3.3 where solutions transition between unimodal and type I bimodal solutions. Theorem 3.4 as well as identifying a singular fold bifurcation between the unimodal and type II bimodal solutions also identifies a curve of parameter values at which a codimension-two singular cusp bifurcation occurs. The fold bifurcation unfolds at this bifurcation and there is a transition between unimodal and type II bimodal solutions without a fold in the bifurcation branch.

The definition of singular solution introduced above, and the resulting solutions found are only useful if they tell us something about the dynamics of (1.1) when $0 < \varepsilon \ll 1$. In the case of one delay (1.3), Mallet-Paret and Nussbaum [30] proved the existence for $\varepsilon > 0$ of a singular solution which is a perturbation of the sawtooth profile. It is not readily apparent

how to extend that proof to the two delay DDE (1.1). So in Sect. 4 we perform a numerical investigation of (1.1) with $1 \gg \varepsilon > 0$ close to the singular limit. We use DDEBiftool [11] to construct bifurcation diagrams and show numerically that there are periodic solutions of (1.1) for $0 < \varepsilon \ll 1$ which are perturbations of the unimodal and type I and II bimodal solutions that we constructed in Sect. 2. Moreover, we find fold bifurcations close to the values predicted by our singular solutions. We also investigate multimodal solutions, which are more complex than the singular solutions that we constructed algebraically. The existence of these seems to be generic on the unstable legs of the branches between folds.

In Sect. 5 we investigate the first two codimension-two cusp-like bifurcations identified in Theorem 3.4. For $0 < \varepsilon \ll 1$ we find cusp bifurcations very close to the values predicted by the singular theory. We also show that these cusp bifurcations provide one mechanism by which stable bimodal periodic solutions may arise, and identify differences between the first and second cusp bifurcation.

In Sect. 6, guided by our results from Sect. 3 we investigate other periodic solutions of (1.1) for $0 < \varepsilon \ll 1$. For $A < 3$ when folds do not occur, we find an unbounded leg of stable type II bimodal solutions, and also period-doubling bifurcations, leading to stable period-doubled orbits. We also show an example of multimodal solutions with fold bifurcations which are associated with transitions between such solutions. We also consider the alignment of the fold bifurcations on different solution branches and explain this using our results from Sect. 3. We finish in Sect. 7 with brief conclusions.

2 Singular Solutions

Before constructing singular solutions for (1.1), as an illustrative example we consider the singular solutions of the one delay DDE (1.3) which we write as

$$\varepsilon \dot{u}(t) = -u(t) - Ku(\alpha(t, u(t))), \quad \alpha(t, u(t)) = t - a_1 - cu(t). \tag{2.1}$$

We will construct periodic singular solutions following Definition 1.2 for (2.1) when $K > 1$ (required for instability of the trivial solution), with the profile below. Here, and throughout we use $\mathbb{N}_0$ to denote the natural numbers including zero.

Definition 2.1 (Sawtooth profile) For any $n \in \mathbb{N}_0$ and period $T > 0$ the *sawtooth profile* is an admissible periodic singular solution profile on $I = \mathbb{R}$ defined by

$$\left.\begin{aligned} t(\mu) &= (\mu - i)T \\ u(\mu) &= \frac{-a_1 + (n + \mu - 2i)T}{c} \end{aligned}\right\} \quad \mu \in [2i, 2i+1], \tag{2.2}$$

$$\left.\begin{aligned} t(\mu) &= (i+1)T \\ u(\mu) &= \frac{-a_1 + (n + 1 - (\mu - 2i - 1))T}{c} \end{aligned}\right\} \quad \mu \in ((2i+1), (2i+2)), \tag{2.3}$$

for each $i \in \mathbb{Z}$.

Figure 1 shows a part of this profile when $a_1 = c = 1$. Notice that I^* is the union of the intervals $(2i, 2i+1)$ and on each such interval u increases from $(-a_1 + nT)/c$ to $(-a_1 + (n+1)T)/c$ while t increases by T. I^- is the union of the intervals $[2i+1, 2i+2]$ and on each such interval u decreases from $(-a_1 + (n+1)T)/c$ to $(-a_1 + nT)/c$ while t is fixed. Mallet-Paret and Nussbaum have considered this Γ (but not our parametrisation of it) extensively, and named it the "sawtooth profile" for the shape of Γ in Fig. 1b [30,31].

The motivation for Definition 2.1 comes from numerical simulations, where we observe when $\dot{u}(t)$ is finite that $\alpha(t,u(t))$ is (almost) constant. The sawtooth profile can then be constructed for (1.3) by assuming that $\alpha(t,u(t))$ is constant with $\alpha(t,u(t)) \in t(I^-)$ when $\dot{u}(t)$ is finite (that is $u(t) \in \Gamma^*$). If the phase of the periodic solution is chosen so that $t(I^-) = \{jT : j \in \mathbb{Z}\}$ then for $t \in (0,T)$ we have $-nT = \alpha(t,u(t)) = t - a_1 - cu(t)$ for some $n \in \mathbb{N}_0$. Rearranging this leads to the formula for u in (2.2) with $i = 0$.

Each different n will define a different singular solution, with delay $t - \alpha(t,u(t)) = a_1 + cu(t) \in [nT,(n+1)T]$. Here we will construct singular solutions of (2.1) for all $n \in \mathbb{N}_0$ with period T given by

$$T = \frac{a_1(1+K)}{1+n(1+K)}. \tag{2.4}$$

Later, we will construct periodic singular solutions of the two delay equation (1.1) using the same sawtooth admissible solution profile. To define a singular solution for (2.1) with this profile, for $j \in \mathbb{Z}$ let

$\mu_0(\eta) =$	$\mu_1(\eta) =$	$\eta \in$
$2j + (\eta - 3j)$	$2(j-n) - 1 + [(\eta - 3j) + (K-1)]/K$	$[3j, 3j+1]$
$2j + 1 + (\eta - 3j - 1)$	$2(j-n) + (\eta - 3j - 1)$	$[3j+1, 3j+2]$
$2j + 2$	$2(j-n) + 1 + (\eta - 3j - 2)(K-1)/K$	$[3j+2, 3j+3]$

(2.5)

Then $\mu_i(\eta)$ is continuous on the real line. It is a simple but tedious algebraic exercise to check that (1.5) holds for all $\eta \in \mathbb{R}$. Notice in particular that for $\eta \in [3j, 3j+1]$ we have $\mu_1(\eta) \in \big(2(j-n)-1, 2(j-n)\big)$ provided $K > 1$, in which case

$$t(\mu_1(\eta)) = (j-n)T = t(\mu_0(\eta)) - a_1 - cu(\mu_0(\eta)) = \alpha\big(t(\mu_0(\eta)), u(\mu_0(\eta))\big),$$

as required to satisfy (1.5). Before checking the conditions on $F(\eta)$, notice that $\mu_0(\eta) \in I^*$ for $\eta \in (3j, 3j+1)$, $\mu_0(\eta) \in \text{int}(I^-)$ for $\eta \in (3j+1, 3j+2)$ and $\mu_0(\eta) \in \partial I^* = \partial I^-$ for $\eta \in [3j+2, 3j+3]$ for each $j \in \mathbb{Z}$. Hence J^* is the union of the intervals $[3j, 3j+1]$, while J^- is composed of intervals $(3j+1, 3j+3)$. For $\eta \in J^*$ we have $F(\eta) = 0$ provided (2.4) holds (which is how T was actually determined). For $\eta \in (3j+1, 3j+2]$ we have

$$\begin{aligned} F(\eta) &= -u(\mu_0(\eta)) - Ku(\mu_1(\eta)) \\ &= -\left[\frac{-a_1 + (n+3j+2)T - \eta T}{c}\right] - K\left[\frac{-a_1 + (n-3j+1)T + \eta T}{c}\right] \\ &= \frac{1}{c}(a_1 - nT)(1+K) - \frac{T}{c} + \frac{1}{c}\big(\eta - (3j+1)\big)T(1-K) \\ &= \frac{1}{c}\big(\eta - (3j+1)\big)T(1-K), \end{aligned}$$

and hence $F(\eta) < 0$ for all $\eta \in (3j+1, 3j+2]$, since $K > 1$. Finally on the interval $[3j+2, 3j+3]$, we have $u(\mu_1(\eta))$ is a linear function of η, while $u(\mu_0(\eta))$ is constant, and hence $F(\eta)$ is a linear function of η. By continuity and the previous calculations $F(3j+2) = T(1-K)/c < 0$ and $F(3j+3) = 0$ hence $F(\eta) < 0$ for all $\eta \in J^-$ as required. Thus for each $n \in \mathbb{N}_0$ and each $K > 1$ we have constructed a periodic singular solution of (2.1) defined by (2.4)–(2.5). The parametrisation leading to one of these solutions and the corresponding periodic singular solution is illustrated in Fig. 2.

Using max-plus equations, in [30] this Γ is proved to be the limiting profile of the slowly oscillating periodic solutions (corresponding to $n = 0$) of (1.3) as $\varepsilon \to 0$. In [31] higher

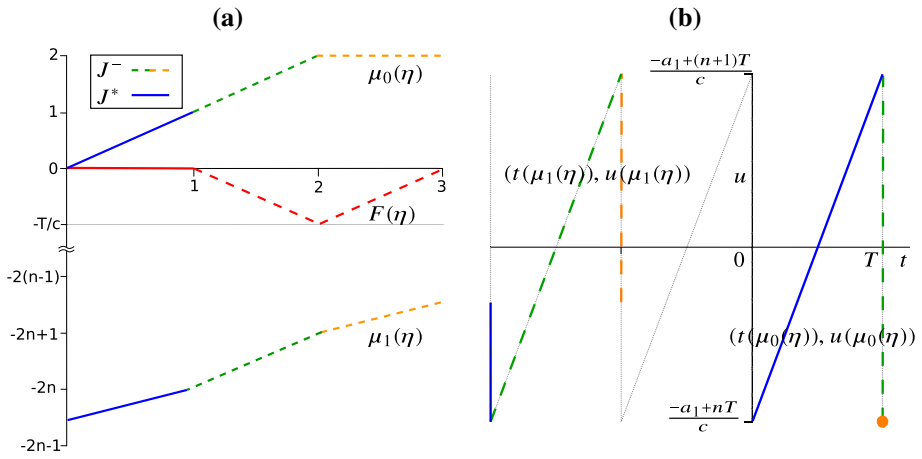

Fig. 2 **a** $\mu_0(\eta)$, $\mu_1(\eta)$ and $F(\eta)$ for $\eta \in [0, 3]$ for the singular solution of (2.1) defined by (2.2)–(2.5). **b** The corresponding periodic singular solution $(t(\mu_0(\eta)), u(\mu_0(\eta)))$ and delayed solution $(t(\mu_1(\eta)), u(\mu_1(\eta)))$ for $\eta \in [0, 3]$

order asymptotics reveal the shape of the periodic solution for $0 < \varepsilon \ll 1$. It is noted that that the asymptotic forms of the periodic solution are very different near to the local maximum and minimum of the solution, with the maximum corresponding to a regular point of the dynamics scaled by ε, while the minimum can be interpreted in the spirit of Fenichel as a turning point near a normally hyperbolic invariant manifold for an ordinary differential equation with a time scaling of ε^2 [31]. The singular solution (2.2)–(2.5) also reveals a difference between the dynamics near to the maximum and minimum of the periodic solution. The solution $u(t(\mu_0(\eta)))$ has its maximum when $\eta = 3j + 1$ (for any integer j), which is at the boundary between two of the linear segments in the solution parametrisation (2.5), corresponding to the boundary between J^* and J^-. In contrast $u(t(\mu_0(\eta)))$ takes its minimum value on the entire interval $\eta \in [3j + 2, 3j + 3]$ (but $u(t(\mu_1(\eta)))$ is not constant on this interval). Note that while at first sight it may have appeared more natural in Definition 1.2 to define J^* to be the set of $\eta \in J$ such that $\mu_0(\eta) \in I^*$ (or equivalently such that $u(\mu_0(\eta)) \in \Gamma^*$), such a definition would be problematical in the example above because $\mu_0(\eta)$ is constant on ∂I^* on the interval $\eta \in [3j + 2, 3j + 3]$. We will also find nontrivial intervals on which $\mu_0(\eta)$ is constant on ∂I^* for singular solutions of (1.1).

Now consider the two delay DDE (1.1). We assume several conditions on the positive parameters. Without loss of generality let $a_2 > a_1$ (otherwise either swap the order of the terms, or reduce to a one delay DDE). Then letting $\alpha_i(t, u(t)) = t - a_i - cu(t)$ we have $\alpha_2(t, u(t)) < \alpha_1(t, u(t))$ with $\alpha_1(t, u(t)) - \alpha_2(t, u(t)) = a_2 - a_1 > 0$, constant. So although $\alpha_i(t, u(t))$ are both linearly state-dependent, their difference is constant. The more general case where $\alpha_i(t, u(t)) = t - a_i - c_i u(t)$ with $c_1 \neq c_2$ so that the difference between the delays is nonconstant would also be interesting, but in the current work we concentrate on understanding the simpler case, which already leads to very complicated dynamics.

It is useful to define the ratio $A = a_2/a_1 > 1$ which will play an important role later. If $K_1 + K_2 < 1$ the trivial solution is asymptotically stable and there are no stable periodic solutions, so we assume that $K_1 + K_2 > 1$. Finally we assume that

$$K_2 < 1. \tag{2.6}$$

It is shown in [19] that $A > 1$ and (2.6) ensure that the DDE initial value problem (IVP) is well-posed for (1.1), and in particular that the delay $\alpha_1(t, u(t))) < t$ and so does not become advanced. It is also shown in [19] for $\varepsilon > 0$ that $\alpha_i(t, u(t)))$ is a strictly monotonic increasing function of t for $t \geqslant t_0 + a_2 + a_1(K_1 + K_2)$, where t_0 is the initial time for the IVP. Hence $\alpha_i(t, u(t)))$ must be a strictly monotonic increasing function of t on any periodic solution. Thus we will construct singular periodic solutions of (1.1) for which $\mu_i(\eta)$ are monotonic increasing functions of η for all i, although Definition 1.2 only requires that $\mu_0(\eta)$ be monotonic in general for (1.2).

We first construct singular periodic solutions for (1.1) which have the same sawtooth profile (2.2), (2.3) as the sawtooth solutions of the one delay DDE (1.3). Since these solutions have one local maxima per period we refer to them as unimodal. We will then construct two types singular periodic solution with two local maxima per step; type I and type II bimodal solutions. Each of the solutions that we construct of each type will be characterised by a pair (n, m) of non-negative integers which will have the same meaning in each case. The first number n is the integer number of periods in the past that the first delay falls, and the second number m is the integer number of periods between the two delay times $\alpha_1(t, u(t)))$ and $\alpha_2(t, u(t)))$. So for a singular solution of period T we always have

$$t - \alpha_1(t, u(t)) \in [nT, (n+1)T], \quad a_2 - a_1 = \alpha_1(t, u(t)) - \alpha_2(t, u(t)) \in (mT, (m+1)T). \tag{2.7}$$

Or, using the parametrisation,

$$t(\mu_0(\eta)) - t(\mu_1(\eta)) = t(\mu_0(\eta)) - \alpha_1(t(\mu_0(\eta)), u(\mu_0(\eta))) \in [nT, (n+1)T], \quad \forall \eta \in \mathbb{R}, \ n \in \mathbb{N}_0. \tag{2.8}$$

and

$$\begin{aligned} t(\mu_1(\eta)) - t(\mu_2(\eta)) &= \alpha_1(t(\mu_0(\eta)), u(\mu_0(\eta))) - \alpha_2(t(\mu_0(\eta)), u(\mu_0(\eta))) \\ &= \big[t(\mu_0(\eta)) - a_1 - cu(\mu_0(\eta))\big] - \big[t(\mu_0(\eta)) - a_2 - cu(\mu_0(\eta))\big] \\ &= a_2 - a_1 \in (mT, (m+1)T), \quad \forall \eta \in \mathbb{R}, \ m \in \mathbb{N}_0. \end{aligned} \tag{2.9}$$

With n and m defined by (2.8) and (2.9) to construct unimodal singular solutions of (1.1) it is useful to define $\theta \in (0, 1)$ by

$$t(\mu_1(\eta)) - t(\mu_2(\eta)) = a_2 - a_1 = (m + \theta)T, \quad \theta \in (0, 1),$$

so θ is the fractional part of a period between the two delays, which is assumed to be non-zero. (Although n and m will always have the same meaning, θ will be defined slightly differently for each type of bimodal solution.) As in the one delay case we will construct a solution with $t(\mu_1(\eta)) = -nT$ while $t(\mu_0(\eta)) \in (0, T)$. The following theorem establishes conditions for such a solution to exist.

Theorem 2.2 *Let $K_1 > 1 > K_2 > 0$, $a_2 > a_1 > 0$, $m, n \in \mathbb{N}_0$,*

$$T = \frac{a_1(1 + K_1 + K_2) + (a_2 - a_1)K_2}{1 + (m+1)K_2 + n(1 + K_1 + K_2)}, \tag{2.10}$$

and

$$\theta = \frac{a_2 - a_1}{T} - m. \tag{2.11}$$

The DDE (1.1) has a periodic singular solution with profile (2.2), (2.3) and period $T > 0$ given by (2.10) when the parameters are chosen so that

$$\theta \in \left(\frac{K_2}{K_1 + K_2 - 1}, 1\right). \tag{2.12}$$

Table 1 Parameterization of the unimodal solution defined in Theorem 2.2 for the sawtooth profile given in Definition 2.1

$\mu_0(\eta) =$	$\mu_1(\eta) =$	$\mu_2(\eta) =$	$\eta \in$
$2j+\eta-5j$	$2j-2n+(-1+\eta-5j)/K_1$	$2(j-n-m)-1-\theta$	$[5j, 5j+1]$
$2j+1+(\eta-5j-1)\theta$	$2(j-n)+(\eta-5j-1)\theta$	$2(j-n-m)-1-\theta+(\eta-5j-1)\theta$	$[5j+1, 5j+2]$
$2j+1+\theta$	$2(j-n)+\theta$	$2(j-n-m)-1+(\eta-5j-2)$	$[5j+2, 5j+3]$
$2j+1+\theta+(\eta-5j-3)(1-\theta)$	$2(j-n)+\theta+(\eta-5j-3)(1-\theta)$	$2(j-n-m)+(\eta-5j-3)(1-\theta)$	$[5j+3, 5j+4]$
$2j+2$	$2(j-n)+1+(1-1/K_1)(\eta-5j-4)$	$2(j+1-n-m)-1-\theta$	$[5j+4, 5j+5]$

Proof For $j \in \mathbb{Z}$ let $\mu_i(\eta)$ be defined by Table 1. By the conditions of the theorem, $\theta \in (0, 1)$ and $K_1 > 1$. From this it follows that each $\mu_i(\eta)$ is continuous and monotonically increasing. For $\eta \in [5j+k, 5j+k+1]$ for $k = 0, 1, 2, 3, 4$, notice that each function $\mu_i(\eta)$ is linear in η, and falls into a single subinterval of the sawtooth profile defined by (2.2), (2.3), and so $u(\mu_i(\eta))$ and $t(\mu_i(\eta))$ are linear functions for $\eta \in [5j+k, 5j+k+1]$. It follows that $F(\eta)$ is also linear in η for $\eta \in [5j+k, 5j+k+1]$ for each integer k. It is straightforward to confirm that (1.5) holds, that is $t(\mu_i(\eta)) = t(\mu_0(\eta)) - a_i - cu(\mu_0(\eta))$ for $i = 1, 2$.

It remains to establish the conditions on F. First note that $J^* = \bigcup_{j\in\mathbb{Z}}[5j, 5j+1]$. Now

$$\begin{aligned} F(5j) &= -u(\mu_0(5j)) - K_1u(\mu_1(5j)) - K_2u(\mu_2(5j)) \\ &= -u(2j) - K_1u(2j-2n-1/K_1) - K_2u(2(j-n-m)-1-\theta) \\ &= -\Big(\frac{-a_1+nT}{c}\Big) - K_1\Big(\frac{-a_1+(n+1/K_1)T}{c}\Big) - K_2\Big(\frac{-a_1+(n+1-\theta)T}{c}\Big) \end{aligned}$$

hence

$$cF(5j) = (a_1 - nT)(1 + K_1 + K_2) - T - (1-\theta)K_2T.$$

But multiplying (2.10) by its denominator, and noting that from (2.11) we have $a_2 - a_1 = (m+\theta)T$, we see that

$$(a_1 - nT)(1 + K_1 + K_2) = -(a_2 - a_1)K_2 + T + (m+1)K_2T = T + (1-\theta)K_2T,$$

and hence $F(5j) = 0$. It follows similarly that $F(5j+1) = 0$, and hence by linearity, $F(\eta) = 0$ for all $\eta \in [5j, 5j+1]$ and hence for all $\eta \in J^*$.

It remains to show that $F(\eta) < 0$ for $\eta \in J^- = \bigcup_{j\in\mathbb{N}}(5j+1, 5j+5)$. Since $F(5j) = F(5j+1) = F(5j+5) = 0$, by the linearity of $F(\eta)$ on each subinterval, it is sufficient to show that $F(5j+2) < 0$, $F(5j+3) < 0$ and $F(5j+4) < 0$. But similarly to above we derive

$$cF(5j+2) = (1 - K_1 - K_2)\theta T, \quad cF(5j+4) = (1-K_1)T,$$

which are both negative since $K_1 > 1$, while

$$cF(5j+3) = cF(5j+2) + K_2T = \big[K_2 - (K_1 + K_2 - 1)\theta\big]T, \tag{2.13}$$

and $F(5j+3) < 0$ provided $\theta > K_2/(K_1 + K_2 - 1)$. Hence $F(\eta) < 0$ for all $\eta \in J^-$, which completes the proof. □

Theorem 2.2 shows immediately that θ is bounded away from zero. We will see in Sect. 3 that only certain pairs of values of $m, n \in \mathbb{N}_0$ satisfy the bounds (2.12) in Theorem 2.2. In Theorem 3.1 we will determine which pairs (n, m) are possible and for which parameter ranges the conditions of Theorem 2.2 are satisfied to begin to construct a bifurcation diagram of solution branches. For now, we note that using (2.10) and (2.11) we can write

$$m + \theta = \frac{(A-1)\big(1 + (m+1)K_2 + n(1+K_1+K_2)\big)}{1 + K_1 + K_2 + (A-1)K_2},$$

where $A = a_2/a_1$. Using this, the condition $\theta > K_2/(K_1 + K_2 - 1)$ can be rewritten as

$$G_{\mathrm{nm}}(K_1) < 0, \tag{2.14}$$

where

$$\begin{aligned} G_{nm}(K_1) = {} & \big[m - n(A-1)\big]\big((K_1+K_2)^2 - 1\big) - K_1\big[(A-1)(1+K_2) - K_2\big] \\ & + K_2(1+K_2) + (A-1). \end{aligned} \tag{2.15}$$

When the parameters are such that the bounds on θ in (2.12) are violated other types of singular solution arise. We will construct two such classes of solutions which we refer to as type I and type II bimodal solutions, since each has two local maxima per period.

Let $n \in \mathbb{N}_0$ and $m \in \mathbb{N}_0$ be related to the delays and period T as explained in (2.7)–(2.9). For $\theta \in (0, 1)$, $T = T_1 + T_2$ where $T_i > 0$, the Type I and Type II bimodal periodic admissible singular solution profiles are defined by

$t(\mu) =$	$u(\mu) =$	$\mu \in$
$(\mu - 4i)T_1 + iT$	$\frac{1}{c}(-a_1 + nT + (\mu - 4i)T_1)$	$[4i, 4i+1]$
$T_1 + iT$	$\frac{1}{c}(-a_1 + nT + T_1 - (\mu - 4i - 1)(T_2 + \theta T_1)$	$[4i+1, 4i+2]$
$(\mu - 4i - 2)T_2 + T_1 + iT$	$\frac{1}{c}(-a_1 + nT + (1-\theta)T_1 + (\mu - 4i - 3)T_2)$	$[4i+2, 4i+3]$
$(i+1)T$	$\frac{1}{c}(-a_1 + nT + (4i + 4 - \mu)(1-\theta)T_1)$	$[4i+3, 4i+4]$,

(2.16)

and

$t(\mu) =$	$u(\mu) =$	$\mu \in$
$(\mu - 4i)T_1 + iT$	$\frac{1}{c}(-a_1 + nT + (\mu - 4i)T_1)$	$[4i, 4i+1]$
$T_1 + iT$	$\frac{1}{c}(-a_1 + nT + T_1 - (\mu - 4i - 1)\theta T_2)$	$[4i+1, 4i+2]$
$(\mu - 4i - 2)T_2 + T_1 + iT$	$\frac{1}{c}(-a_1 + nT + T_1 - \theta T_2 + (\mu - 4i - 2)T_2)$	$[4i+2, 4i+3]$
$(i+1)T$	$\frac{1}{c}(-a_1 + nT + (T - \theta T_2)(4i + 4 - \mu))$	$[4i+3, 4i+4]$,

(2.17)

respectively. These profiles are illustrated in Figs. 3 and 4.

We see from the (2.16) and (2.17) that both solutions have global minima with $u = (-a_1 + nT)/c$. If the phase of the periodic solution is chosen so that these minima occur when $t = jT$, for integer j, then for type I bimodal solutions the first local maximum which occurs when $t = jT + T_1$ is also the global maximum, while for type II bimodal solutions the second local maximum on the period is equal to the global maximum.

The following theorem identifies all the conditions on the parameters for a type I bimodal solution to exist. In Theorem 3.3 we find parameter ranges for which all these conditions are satisfied. The integers n and m in Theorem 2.3 have similar geometrical meanings as for the

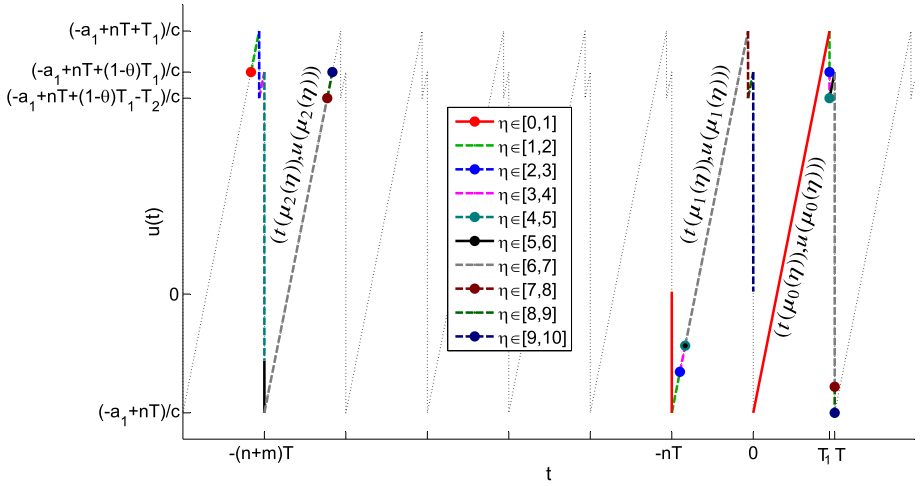

Fig. 3 A generic Type I admissible bimodal periodic solution profile as defined in (2.16). Also shown in colour are the ten stages of the parametrisation of $(t(\mu_i(\eta)), u(\mu_i(\eta)))$ from the proof of Theorem 2.3 for $i = 0, 1, 2$ and $j = 0$. Where plotted the *dots* indicate that $(t(\mu_i(\eta)), u(\mu_i(\eta)))$ is constant for that stage of the parametrisation, with the *multicoloured dot* showing that $(t(\mu_1(\eta)), u(\mu_1(\eta)))$ is constant for two successive stages for $\eta \in [4, 6]$ (Color figure online)

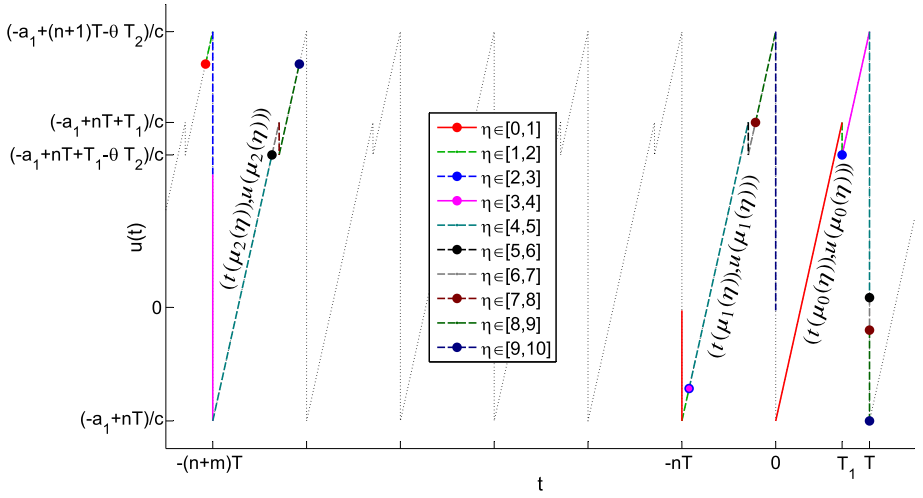

Fig. 4 A generic Type II admissible bimodal periodic solution profile as defined in (2.17). Also shown in *colour* are the ten stages of the parametrisation of $(t(\mu_i(\eta)), u(\mu_i(\eta)))$ from the proof of Theorem 2.4 for $i = 0, 1, 2$ and $j = 0$ (Color figure online)

sawtooth solution, so n and m again satisfy (2.7)–(2.9). For the type I bimodal solution it is convenient to define $\theta \in (0, 1)$ by $a_2 - a_1 = mT + T_2 + \theta T_1$ where $m \in \mathbb{N}_0$, $\theta \in (0, 1)$ and $T = T_1 + T_2$ so

$$\begin{aligned} t(\mu_1(\eta)) - t(\mu_2(\eta)) &= \alpha_1(t(\mu_0(\eta)),\ u(\mu_0(\eta))) - \alpha_2(t(\mu_0(\eta)), u(\mu_0(\eta))) \\ &= a_2 - a_1 = mT + T_2 + \theta T_1 \in (mT + T_2, (m + 1)T). \end{aligned}$$

Thus when $\alpha_1(t(\mu_0(\eta)), u(\mu_0(\eta))) = t(\mu_1(\eta)) = -nT$ we have

$$\begin{aligned}\alpha_2(t(\mu_0(\eta)),\ u(\mu_0(\eta))) &= t(\mu_2(\eta)) = -(n+m)T - T_2 - \theta T_1\\ &= -(n+m+1)T + (1-\theta)T_1 \in [-(n+m+1)T, -(n+m+1)T + T_1]\end{aligned}$$

and the second delay falls in the first leg of the periodic solution. The condition $T_2 + \theta T_1 < T_1$ which is implied by the conditions of Theorem 2.3 ensures that when the second delay satisfies $\alpha_2(t(\mu_0(\eta)), u(\mu_0(\eta))) = t(\mu_2(\eta)) = -(n+m)T$ the first delay satisfies $\alpha_1(t(\mu_0(\eta)), u(\mu_0(\eta))) = t(\mu_1(\eta)) = -nT + T_2 + \theta T_1 \in (-nT, -nT + T_1)$ and hence also falls in the first leg of the periodic solution.

Theorem 2.3 *Let $K_1 > 1 > K_2 > 0$ and define*

$$T = \frac{a_1(1 + K_1 + K_2) + (a_2 - a_1)(1 - K_1)}{1 - m(K_1 - 1) + n(1 + K_1 + K_2)}, \tag{2.18}$$

and

$$T_2 = \frac{a_1 G_{nm}(K_1)}{1 - m(K_1 - 1) + n(1 + K_1 + K_2)} \tag{2.19}$$

where $G_{nm}(K_1)$ is defined by (2.15), and $T_1 = T - T_2$. Let the parameters be chosen so that $T_2 > 0$,

$$\theta := \frac{a_2 - a_1 - mT - T_2}{T_1}, \tag{2.20}$$

satisfies $\theta \in (0, 1 - 1/K_1)$ and

$$\frac{K_2}{K_1 - 1} T_2 < \theta T_1 < T_1 - \frac{1}{K_2} T_2, \tag{2.21}$$

then (1.1) has a Type I bimodal singular solution of period $T > 0$ with solution profile given by (2.16).

Proof Note that the upper bound on θT_1 implies that $T_2 < K_2(1 - \theta)T_1$. Hence $0 < T_2 < T_1 < T_1 + T_2 = T$, and $T_2 + \theta T_1 < T_1$ (since $K_2 < 1$). It is also useful to notice that (2.18) can be rearranged as

$$T = (a_1 - nT)(1 + K_1 + K_2) + (1 - K_1)(a_2 - a_1 - mT) \tag{2.22}$$

and (2.20) as

$$a_2 - a_1 - mT = T_2 + \theta T_1. \tag{2.23}$$

Now for $j \in \mathbb{Z}$ let the functions $\mu_i(\eta)$ for $i = 0, 1, 2$ be defined by Table 2 where

$$s_{11} = \frac{\theta T_1}{T_2 + \theta T_1}, \quad s_{12} = 1 - \frac{T_2}{(1-\theta)T_1}, \quad s_{13} = 1 - \frac{1}{K_1(1-\theta)}, \quad s_{14} = 1 - \frac{T_2}{K_2(1-\theta)T_1}. \tag{2.24}$$

Clearly $s_{11} \in (0, 1)$, while $1 > s_{12} > s_{14} > 0$, where the last inequality follows from the upper bound on θT_1 in (2.21). The bound $\theta < 1 - 1/K_1$ also implies that $s_{13} \in (0, 1)$. It follows that each $\mu_i(\eta)$ is continuous and monotonically increasing. Moreover for $\eta \in [10j + k, 10j + k + 1]$ with k a non-negative single digit integer each function $\mu_i(\eta)$ is linear in η with range contained in an interval on which $u(\mu)$ and $t(\mu)$ defined by (2.16) are linear. It follows that $t(\mu_i(\eta))$ and $u(\mu_i(\eta))$ are linear functions of η for $\eta \in [10j + k, 10j + k + 1]$, for integers j and non-negative single digit integers k, as illustrated in the colour version of Fig. 3 with $j = 0$. It then follows that $F(\eta)$ is linear on each subinterval $\eta \in [10j + k, 10j + k + 1]$.

Table 2 Parameterization of the type I bimodal solution defined in Theorem 2.3 for the admissible profile defined by (2.16), illustrated in Fig. 3

$\mu_0(\eta) =$	$\mu_1(\eta) =$	$\mu_2(\eta) =$	$\eta \in$
$4j + (\eta - 10j)$	$4(j-n) - 1 + s_{13} + (1 - s_{13})(\eta - 10j)$	$4(j-n-m) - 3 - \theta$	$[10j, 10j + 1]$
$4j + 1 + (\eta - 10j - 1)s_{11}$	$4(j-n) + (\eta - 10j - 1)\theta$	$4(j-n-m) - 3 - \theta + (\eta - 10j - 1)\theta$	$[10j + 1, 10j + 2]$
$4j + 1 + s_{11}$	$4(j-n) + \theta$	$4(j-n-m) - 3 + (\eta - 10j - 2)$	$[10j + 2, 10j + 3]$
$4j + 2 + (\eta - 10j - 4)(1 - s_{11})$	$4(j-n) + \theta + (\eta - 10j - 3)T_2/T_1$	$4(j-n-m) - 2 + (\eta - 10j - 3)$	$[10j + 3, 10j + 4]$
$4j + 2$	$4(j-n) + \theta + T_2/T_1$	$4(j-n-m) - 1 + (\eta - 10j - 4)s_{14}$	$[10j + 4, 10j + 5]$
$4j + 2 + (\eta - 10j - 5)$	$4(j-n) + \theta + T_2/T_1$	$4(j-n-m) + (-1 + \eta - 10j - 5)(1 - s_{14})$	$[10j + 5, 10j + 6]$
$4j + 3 + (\eta - 10j - 6)s_{12}$	$4(j-n) + 1 + (\eta - 10j - 7)(1 - \theta - T_2/T_1)$	$4(j-n-m) + (1 - \theta - T_2/T_1)(\eta - 10j - 6)$	$[10j + 6, 10j + 7]$
$4j + 3 + s_{12}$	$4(j-n) + 1 + (\eta - 10j - 7)$	$4(j-n-m) + 1 - \theta - T_2/T_1$	$[10j + 7, 10j + 8]$
$4(j+1) + (\eta - 10j - 9)(1 - s_{12})$	$4(j-n) + 2 + (\eta - 10j - 8)$	$4(j-n-m) + 1 - \theta + T_2/T_1(\eta - 10j - 9)$	$[10j + 8, 10j + 9]$
$4(j+1)$	$4(j-n) + 3 + (\eta - 10j - 9)s_{13}$	$4(j+1-n-m) - 3 - \theta$	$[10j + 9, 10(j+1)]$

It is straightforward to verify that (1.5) holds, that is $t(\mu_i(\eta)) = t(\mu_0(\eta)) - a_i - cu(\mu_0(\eta))$ for $i = 1, 2$ for all $\eta \in [10j, 10(j+1)]$ and hence for all $\eta \in \mathbb{R}$.

It remains only to verify the conditions on F. First note that $J^* = \bigcup_j [10j, 10j + 1] \cup [10j + 5, 10j + 6]$, which defines the intervals on which $t(\mu_0(\eta))$ is non-constant. Note also that $t(\mu_1(\eta)) = (j-n)T$ and $t(\mu_2(\eta)) = (j-n-m)T - T_2 - \theta T_1$ for all $\eta \in [10j, 10j+1]$, while $t(\mu_2(\eta)) = (j-n-m)T$ and $t(\mu_1(\eta)) = (j-n)T + T_2 + \theta T_1 \in ((j-n)T, (j-n)T + T_1)$ for all $\eta \in [10j + 5, 10j + 6]$.

When $\eta = 10j + 6$ we have

$$u(\mu_0(10j+6)) = u(4j+3) = \frac{1}{c}(-a_1 + nT + (1-\theta)T_1),$$
$$u(\mu_1(10j+6)) = u(4j - 4n + \theta + T_2/T_1) = \frac{1}{c}(-a_1 + nT + T_2 + \theta T_1),$$
$$u(\mu_2(10j+6)) = u(4j - 4n - 4m) = \frac{1}{c}(-a_1 + nT).$$

Hence

$$\begin{aligned} F(10j+6) &= -u(\mu_0(10j+6)) - K_1 u(\mu_1(10j+6)) - K_2 u(\mu_2(10j+6)) \\ &= -\frac{1}{c}(-a_1 + nT + (1-\theta)T_1) - \frac{K_1}{c}(-a_1 + nT + T_2 + \theta T_1) \\ &\quad - \frac{K_2}{c}(-a_1 + nT). \end{aligned}$$

Thus, since $T = T_1 + T_2$,

$$cF(10j+6) = (a_1 - nT)(1 + K_1 + K_2) - T + (1 - K_1)(T_2 + \theta T_1),$$

and $F(10j+6) = 0$ using (2.22) and (2.23). Similarly, using (2.24),

$$cF(10j+5) = cF(10j+6) + T_2 - K_2(1-\theta)(1-s_{13})T_1 = 0.$$

Hence by the linearity of F we have $F(\eta) = 0$ for all $\eta \in [10j+5, 10j+6]$. Also

$$\begin{aligned} F(10j+1) &= -u(\mu_0(10j+1)) - K_1 u(\mu_1(10j+1)) - K_2 u(\mu_2(10j+1)) \\ &= -\frac{1}{c}(-a_1 + nT + T_1) - \frac{K_1}{c}(-a_1 + nT) - \frac{K_2}{c}(-a_1 + nT + (1-\theta)T_1). \end{aligned}$$

Thus

$$\begin{aligned} cF(10j+1) &= (a_1 - nT)(1 + K_1 + K_2) - T_1 - K_2(1-\theta)T_1, \\ &= (a_1 - nT)(1 + K_1 + K_2) - T_1 - K_2 T + K_2(a_2 - a_1 - mT), \end{aligned}$$

and by (2.22) we find that $F(10j+1) = 0$. Similarly, using (2.24),

$$cF(10j) = cF(10j+1) + T_1\big[1 - K_1(1-\theta)(1-s_{11})\big] = 0.$$

The linearity of $F(\eta)$ for $\eta \in [10j, 10j+1]$, now ensures that $F(\eta) = 0$ for all $\eta \in J^*$.

It remains to show that $F(\eta) < 0$ for all $\eta \in J^-$. Again, calling on the linearity of F on each subinterval, it is sufficient to show that $F(10j+k) < 0$ for $k = 2, 3, 4, 7, 8, 9$. But

$$\begin{aligned} cF(10j+2) &= cF(10j+1) - \theta T_1[K_1 + K_2 - 1] < 0, \\ cF(10j+3) &= cF(10j+1) + (1-K_1)\theta T_1 + K_2 T_2 = (1-K_1)\theta T_1 + K_2 T_2, \\ cF(10j+4) &= cF(10j+3) - (K_1 + K_2 - 1)T_2 < cF(10j+3), \\ cF(10j+7) &= cF(10j+6) - (K_1 + K_2 - 1)((1-\theta)T_1 - T_2) < 0, \\ cF(10j+8) &= cF(10j+3) - (K_1 - 1)(T_1 - T_2) - \theta T_1(1 + 2K_2) < cF(10j+3), \\ cF(10j+9) &= cF(10j+8) - (K_1 + K_2 - 1)T_2) < cF(10j+8), \end{aligned}$$

which establishes all the required conditions if $F(10j+3) < 0$, but this holds because $\theta > \frac{K_2}{K_1 - 1}\frac{T_2}{T_1}$, which completes the proof. □

Next we identify the conditions on the parameters for a type II bimodal solution to exist. In Theorem 3.4 we find parameter ranges for which these conditions are satisfied. The integers n and m have the same geometric meaning as for the unimodal and type I bimodal solutions and hence satisfy (2.7)–(2.9). For the type II bimodal solution we let $a_2 - a_1 = mT + \theta T_2$ where $m \in \mathbb{N}_0$, $\theta \in (0, 1)$ and $T = T_1 + T_2$ so

$$\begin{aligned} t(\mu_1(\eta)) - t(\mu_2(\eta)) &= \alpha_1(t(\mu_0(\eta)), u(\mu_0(\eta))) - \alpha_2(t(\mu_0(\eta)), u(\mu_0(\eta))) \\ &= a_2 - a_1 = mT + \theta T_2 \in (mT, mT + T_2). \end{aligned}$$

Thus when $\alpha_1(t(\mu_0(\eta)), u(\mu_0(\eta))) = t(\mu_1(\eta)) = -nT$ we have

$$\begin{aligned} &\alpha_2(t(\mu_0(\eta)),\ u(\mu_0(\eta))) = t(\mu_2(\eta)) = -(n+m)T - \theta T_2 \\ &= -(n+m+1)T + T_1 + (1-\theta)T_2 \in [-(n+m+1)T + T_1, -(n+m)T] \end{aligned}$$

and the second delay falls in the second leg of the periodic solution, as indicated in Fig. 4. The condition $\theta T_2 < T_1$ which is implied by the conditions of Theorem 2.4 ensures that when the second delay satisfies $\alpha_2(t(\mu_0(\eta)), u(\mu_0(\eta))) = t(\mu_2(\eta)) = -(n+m)T$ the first

delay satisfies $\alpha_1(t(\mu_0(\eta)), u(\mu_0(\eta))) = t(\mu_1(\eta)) = -nT + \theta T_2 \in (-nT, -nT + T_1)$ and hence falls in the first leg of the periodic solution, as illustrated in Fig. 4.

Theorem 2.4 *Let $K_1 + K_2 > 1 > K_2 > 0$, let T be defined by (2.18), let*

$$T_2 = \frac{a_1 H_{nm}(K_1)}{1 - m(K_1 - 1) + n(1 + K_1 + K_2)}, \tag{2.25}$$

where

$$\begin{aligned} H_{nm}(K_1) = &\big[m - n(A-1)\big](K_1 + K_2 + 1)(K_1 + 2K_2 - 1) \\ &- K_1\big[(A-1)(1+K_2) - K_2\big] + K_2(1+K_2) + (A-1)(1-K_2), \end{aligned} \tag{2.26}$$

and $T_1 = T - T_2$. Let the parameters be chosen so that $T_2 > 0$ and $\theta \in (0, 1)$ where

$$\theta = \frac{a_2 - a_1 - mT}{T_2}, \tag{2.27}$$

satisfies $\theta < \frac{T_1}{T_2} + 1 - \frac{1}{K_2}$ and if $K_1 \geqslant 1$

$$\theta < \left(1 - \frac{1}{K_1 + K_2}\right)\frac{T_1}{T_2}, \tag{2.28}$$

or if $K_1 < 1$ then

$$\theta < \min\left\{1 - \frac{(1-K_1)}{K_1}\frac{T_1}{T_2}, \left(1 - \frac{K_1}{2K_1 + K_2 - 1}\right)\frac{T_1}{T_2}\right\}. \tag{2.29}$$

Then (1.1) has a Type II bimodal singular solution of period $T > 0$ with solution profile given by (2.17).

Proof This proof is similar to the proof of Theorem 2.3, differing only in the details and conditions, due to differences in the solution profiles and parameterisations. First note that (2.22) is also valid for this solution, while (2.27) can be rewritten as

$$a_2 - a_1 - mT = \theta T_2. \tag{2.30}$$

Also $\theta < \frac{T_1}{T_2} + 1 - \frac{1}{K_2}$ implies that $\theta T_2 < T_1$ and hence $0 < T_1 < T$. Now, for $j \in \mathbb{Z}$ define $\mu_i(\eta)$ by Table 3 where

$$\begin{aligned} s_{21} = \frac{T_1 - \theta T_2}{T - \theta T_2},\ s_{22} = \frac{T - T_2}{T - \theta T_2},\ s_{23} = 1 - \frac{T_1}{K_1(T_1 + (1-\theta)T_2)}, \\ s_{24} = 1 - \frac{T_2}{K_2(T_1 + (1-\theta)T_2)}. \end{aligned} \tag{2.31}$$

Then $1 > s_{22} > s_{21} > 0$ and clearly $s_{23} < 1$ and $s_{24} < 1$. If $K_1 \geqslant 1$ then $s_{23} > 0$, while if $K_1 < 1$ we require $\theta < 1 - \frac{(1-K_1)T_1}{K_1 T_2}$ for $s_{23} > 0$. Finally $\theta < \frac{T_1}{T_2} + 1 - \frac{1}{K_2}$ implies that $s_{24} > 0$. Under these conditions $s_{2j} \in (0, 1)$ for all j and it follows that each $\mu_i(\eta)$ is continuous and monotonically increasing. Moreover for $\eta \in [10j + k, 10j + k + 1]$ with k a non-negative single digit integer each function $\mu_i(\eta)$ is linear in η with range contained in an interval on which $u(\mu)$ and $t(\mu)$ defined by (2.17) are linear, as illustrated in Fig. 4. It follows that $F(\eta)$ is linear on each subinterval $\eta \in [10j + k, 10j + k + 1]$. It is straightforward to verify that (1.5) holds, that is $t(\mu_i(\eta)) = t(\mu_0(\eta)) - a_i - cu(\mu_0(\eta))$ for $i = 1, 2$.

Table 3 Parameterization of the type II bimodal solution defined in Theorem 2.4 for the admissible profile defined by (2.17), illustrated in Fig. 4

$\mu_0(\eta) =$	$\mu_1(\eta) =$	$\mu_2(\eta) =$	$\eta \in$
$4j + (\eta - 10j)$	$4(j-n) + (-1 + \eta - 10j)(1 - s_{23})$	$4(j-n-m) - 1 - \theta$	$[10j, 10j+1]$
$4j+1+(\eta-10j-1)$	$4(j-n) + (\eta-10j-1)\theta T_2/T_1$	$4(j-n-m) - 1 - \theta + \theta(\eta - 10j - 1)$	$[10j+1, 10j+2]$
$4j+2$	$4(j-n) + \theta T_2/T_1$	$4(j-n-m) - 1 + (\eta - 10j - 2)s_{24}$	$[10j+2, 10j+3]$
$4j+2+(\eta-10j-3)$	$4(j-n) + \theta T_2/T_1$	$4(j-n-m) + (\eta-10j-4)(1-s_{24})$	$[10j+3, 10j+4]$
$4j+3+(\eta-10j-4)s_{21}$	$4(j-n)+1+(1-\theta T_2/T_1)(\eta-10j-5)$	$4(j-n-m)+(1-\theta T_2/T_1)(\eta-10j-4)$	$[10j+4, 10j+5]$
$4j+3+s_{21}$	$4(j-n)+1+(\eta-10j-5)$	$4(j-n-m)+1-\theta T_2/T_1$	$[10j+5, 10j+6]$
$4j+3+s_{21}+(\eta-10j-6)(s_{22}-s_{21})$	$4(j-n)+2+(\eta-10j-6)\theta$	$4(j-n-m)+1+\theta T_2/T_1(\eta-10j-7)$	$[10j+6, 10j+7]$
$4j+3+s_{22}$	$4(j-n)+2+\theta$	$4(j-n-m)+1+(\eta-10j-7)$	$[10j+7, 10j+8]$
$4(j+1)+(\eta-10j-9)(1-s_{22})$	$4(j-n)+2+\theta+(\eta-10j-8)(1-\theta)$	$4(j-n-m)+2+(1-\theta)(\eta-10j-8)$	$[10j+8, 10j+9]$
$4(j+1)$	$4(j-n)+3+(\eta-10j-9)s_{23}$	$4(j+1-n-m)-1-\theta$	$[10j+9, 10(j+1)]$

It remains only to verify the conditions on F. First note that $J^* = \bigcup_j [10j, 10j+1] \cup [10j+3, 10j+4]$. Now,

$$\begin{aligned} F(10j+4) &= -u(\mu_0(10j+4)) - K_1 u(\mu_1(10j+4)) - K_2 u(\mu_2(10j+4)) \\ &= -\frac{1}{c}(-a_1 + nT + T_1 + (1-\theta)T_2) - \frac{K_1}{c}(-a_1 + nT + \theta T_2) \\ &\quad - \frac{K_2}{c}(-a_1 + nT) \end{aligned}$$

Hence,

$$cF(10j+4) = (a_1 - nT)(1 + K_1 + K_2) - T_1 - (1-\theta)T_2 - K_1\theta T_2,$$

and $F(10j+4) = 0$ using (2.22), (2.30) and $T = T_1 + T_2$. Similarly, using (2.31),

$$cF(10j+3) = cF(10j+4) + T_2 - K_2(T_1 + (1-\theta)T_2)(1 - s_{24}) = 0.$$

Hence by the linearity of F we have $F(\eta) = 0$ for all $\eta \in [10j+3, 10j+4]$. Similarly,

$$\begin{aligned} cF(10j+1) &= (a_1 - nT)(1 + K_1 + K_2) - T_1 - K_2[T_1 + (1-2\theta)T_2] \\ &= (a_1 - nT)(1 + K_1 + K_2) - T_1 - K_2 T + 2K_2(a_2 - a_1 - mT), \end{aligned}$$

and using (2.22) and (2.25) we find that $F(10j+1) = 0$, while, using (2.31),

$$cF(10j) = cF(10j+1) + T_1 - K_1(T_1 + (1-\theta)T_2)(1 - s_{23}) = 0.$$

The linearity of $F(\eta)$ for $\eta \in [10j, 10j+1]$, now ensures that $F(\eta) = 0$ for all $\eta \in J^*$.

It remains only to show that $F(\eta) < 0$ for all $\eta \in J^-$. Again, using linearity on each subinterval, it is sufficient to show that $F(10j+k) < 0$ for $k = 2, 5, 6, 7, 8, 9$. But

$$\begin{aligned}
cF(10j+2) &= cF(10j+1) - (K_1+K_2-1)\theta T_2 < 0,\\
cF(10j+5) &= cF(10j+4) - (K_1+K_2-1)(T_1-\theta T_2) < 0,\\
cF(10j+6) &= -(K_1+K_2-1)(T_1-\theta T_2) + K_1\theta T_2,\\
cF(10j+7) &= cF(10j+8) - K_2\theta T_2 < cF(10j+8),\\
cF(10j+8) &= -(K_1+K_2-1)(T_1-\theta T_2) + \theta T_2,\\
cF(10j+9) &= cF(10j) - S_{23}K_1(T_1+(1-\theta)T_2) < 0.
\end{aligned}$$

Now if $K_1 \geqslant 1$ then $F(10j+8) \leqslant F(10j+6) < 0$ by (2.28) and all required conditions are satisfied for $F(\eta) < 0$ for all $\eta \in J^-$. If $K_1 < 1$ then $F(10j+6) < F(10j+8) < 0$ (using the right-hand inequality in (2.29)), and again $F(\eta) < 0$ for all $\eta \in J^-$. □

For type I bimodal solutions to exist we require $K_1 > 1$ in Theorem 2.3. This condition is used twice in an essential way in the proof of that theorem, to show that $s_{13} > 0$ and also that $F(10j+3) < 0$, and so Type I bimodal solutions can only exist for $K_1 > 1$. In contrast, Theorem 2.4 does not require $K_1 > 1$, and we will see examples later of type II bimodal solutions which exist for $K_1 < 1$.

The type I and type II bimodal solutions were constructed so that when $\alpha_1 = -nT$ the second delay α_2 falls in the first (type I) or second (type II) leg of the periodic solution, and for both solutions when the second delay satisfies $\alpha_2 = -(n+m)T$ the first delay satisfies $\alpha_1 \in (-nT, -nT+T_1)$ so falls in the first leg of the solution. We also investigated solutions where the first delay satisfies $\alpha_1 \in (-nT+T_1, -(n-1)T)$ when $\alpha_2 = -(n+m)T$ and so α_1 falls in the second leg of the solution. However, we did not find examples of such solutions on the branches, so will not present them here.

3 Bifurcation Branches

Theorems 2.2, 2.3 and 2.4 specify parameter conditions for unimodal and Type I and II bimodal singular solutions to exist for (1.1). In this section we use those theorems to construct parts of the bifurcation branches. We require $K_2 < 1$ to ensure that (1.1) is well posed, while K_1 can be arbitrary large. Thus, it is natural to take K_1 as a bifurcation parameter.

The unimodal and type I and type II bimodal solutions will be characterized by a pair of integers (n, m) as in the last section, where n and m are related to the delays via (2.7)–(2.9). We will see that each value of n defines a different branch of solutions, with each branch mainly made up of segments of unimodal and type I and II bimodal singular solutions for certain values of m. An example is shown in Fig. 5. To explain this example we need to study the parameter conditions from the three aforementioned theorems more closely.

First consider the bounds (2.12) on θ from Theorem 2.2 for the existence of unimodal solutions. By (2.11), the bound $\theta < 1$ is equivalent to $a_2 - a_1 < (m+1)T$. Using (2.10) with $A = a_2/a_1$ this becomes

$$(A-1)(1+(m+1)K_2+n(1+K_1+K_2)) < (1+m)(1+K_1+K_2+(A-1)K_2),$$

and hence $\theta < 1$ is equivalent to

$$m - n(A-1) > -1 + \frac{A-1}{1+K_1+K_2}. \tag{3.1}$$

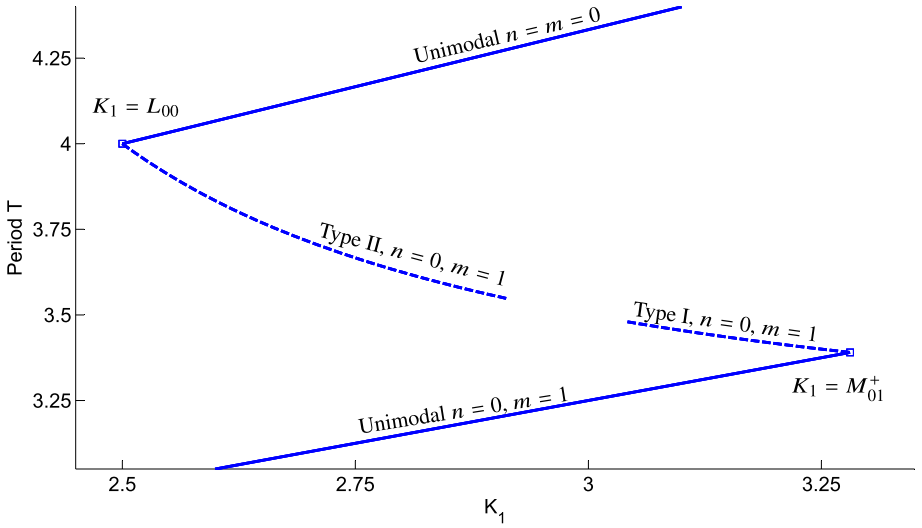

Fig. 5 Example showing periods of unimodal and bimodal solutions satisfying the conditions of Theorems 2.2, 2.3 and 2.4 and forming a branch with two singular fold points at $K_1 = L_{00} = 2.5$ and $K_1 = M_{01}^+ \approx 3.2808$ with $K_2 = 0.5$ and $a_2 = A = 5$ and $a_1 = c = 1$. The apparent gap in the branch near $K_1 = 3$ is studied in Sect. 4

We already showed that the bound $\theta > K_2/(K_1 + K_2 - 1)$ can be written as $G_{nm}(K_1) < 0$ where $G_{nm}(K_1)$ is defined by (2.15). Notice that both bounds only depend on n and m through the common term $m - n(A-1)$. Let us consider the possible values of m and $K_1 > 1$ that satisfy these inequalities for fixed values of the other parameters. First define

$$m^*(n) = n(A-1) + \frac{A-3-K_2}{2+K_2}, \tag{3.2}$$

then when $m \geqslant m^*(n)$ we have

$$m - n(A-1) \geqslant \frac{A-3-K_2}{2+K_2} = -1 + \frac{A-1}{2+K_2} > -1 + \frac{A-1}{1+K_1+K_2},$$

and hence the bound $\theta < 1$ is satisfied for all $K_1 > 1$. If $m \in (n(A-1)-1, m^*(n))$ we find that (3.1) is satisfied for $K_1 > L_{nm}$ where

$$L_{nm} := \frac{A-1}{m - n(A-1) + 1} - (1 + K_2) > 1. \tag{3.3}$$

If $m = m^*(n)$ we have $L_{nm^*} = 1$. Finally there is no unimodal solution satisfying the conditions of Theorem 2.2 if $m \leqslant n(A-1) - 1$, since then it is impossible to satisfy (3.1).

Now to establish an interval of K_1 parameters on which a unimodal solution exists, we need to consider both the bounds $\theta < 1$ and $\theta > K_2/(K_1 + K_2 - 1)$ together. Let $m^0(n)$ be the unique integer for which $m^0(n) \in (n(A-1)-1, n(A-1)]$ and let

$$\begin{aligned} m^{**}(n) = n(A-1) &+ \frac{1}{2}\big[(A-1)\big((1+K_2)^2 - K_2\big) + K_2\big] \\ &- \frac{1}{2}\sqrt{\big(1+(1+K_2)^2\big)\big(((A-1)K_2+1)^2 - 1\big)} \end{aligned} \tag{3.4}$$

In the following theorem we establish that for $m = m^0(n)$ there is a unimodal solution satisfying the conditions of Theorem 2.2 for all K_1 sufficiently large, while for each integer $m \in (m^0(n), m^{**}(n))$, there is a non-empty bounded interval of values of K_1 for which (1.1) has a unimodal solution.

Theorem 3.1 *Let $A = a_2/a_1 > 1$, $K_2 \in (0, 1)$, and $n \in \mathbb{N}_0$. Let $m^*(n)$, $m^{**}(n)$, L_{nm} be defined by (3.2)–(3.4). When $G_{nm}(K)$ defined by (2.15) has distinct roots denote them as $M^-_{nm} < M^+_{nm}$, and let M_{nm} be the root of $G_{nm}(K)$ when it has a unique root.*

(i) *For $m = m^0(n) \in (n(A-1)-1, n(A-1)]$ there is a unimodal singular solution satisfying the conditions of Theorem 2.2 for all $K_1 > \max\{L_{nm}, M^+_{nm}\}$ for any $A > 1$ if $m^0(n) < n(A-1)$ and for all $K_1 > \max\{L_{00}, M_{00}\}$ when $A > 1 + \frac{K_2}{1+K_2}$ if $m^0(n) = n(A-1)$.*

(ii) *For each integer $m \in (n(A-1), m^*(n))$ Eq. (1.1) has a unimodal singular solution satisfying the conditions of Theorem 2.2 for all $K_1 \in (L_{nm}, M^+_{nm})$ where $1 < L_{nm} < M^+_{nm} < \infty$.*

(iii) *If $m = m^*(n) > m^0(n)$, then (1.1) has a unimodal singular solution satisfying the conditions of Theorem 2.2 for all $K_1 \in (1, M^+_{nm^*})$, where $1 = L_{nm^*} = M^-_{nm^*} < M^+_{nm^*}$.*

(iv) *For each integer $m > m^0(n)$ with $m \in (m^*(n), m^{**}(n))$ when $A > 1 + \frac{K_2}{1+K_2}$ we have $1 \leqslant M^-_{nm} < M^+_{nm} < +\infty$ and (1.1) has a unimodal singular solution satisfying the conditions of Theorem 2.2 for all $K_1 \in (M^-_{nm}, M^+_{nm})$*

(v) *There is no unimodal singular solution satisfying the conditions of Theorem 2.2 if $m < m^0(n)$ or $m \geqslant m^{**}(n)$.*

Proof First consider the case when $m = m^0(n) \in (n(A-1)-1, n(A-1))$. If $m < m^*(n)$ (which is always the case if $A \geqslant 3 + K_2$) then we have $\theta < 1$ for $K_1 > L_{nm} > 1$. Now consider the polynomial $G_{nm}(K_1)$. In this case the coefficient of the quadratic term is negative, and it is easy to verify that $G_{nm}(0) > 0 > G_{nm}(L_{nm})$ and hence $M^+_{nm} < L_{nm}$ and $G_{nm}(K_1) < 0$ for all $K_1 \geqslant L_{nm}$. It follows that (2.12) is satisfied for all $K_1 > L_{nm} > 1$. On the other hand if $m \geqslant m^*(n)$ then $\theta < 1$ is satisfied for all $K_1 > 1 \geqslant L_{nm}$ while the coefficient of the quadratic term of $G_{nm}(K_1)$ is still negative, but now $G_{nm}(1) > 0$. In this case $G_{nm}(K_1) = 0$ has a unique positive root $K_1 = M^+_{nm} > 1$ and (2.12) is satisfied for all $K_1 > M^+_{nm} > 1$.

Next consider the case when $m = m^0(n) = n(A-1)$, which can only arise when A is rational or when $n = 0$. In this case the quadratic term in $G_{nm}(K_1)$ vanishes and the condition $G_{nm}(K_1) < 0$ becomes

$$-K_1\big[(A-1)(1+K_2) - K_2\big] + K_2(1+K_2) + (A-1) < 0, \tag{3.5}$$

which can only be satisfied for $K_1 > 1$ if $A > 1 + \frac{K_2}{1+K_2}$. In that case (3.5) is satisfied for

$$K_1 > M_{00} := \frac{K_2(1+K_2) + A - 1}{(A-1)(1+K_2) - K_2}. \tag{3.6}$$

If we also set $m = n(A-1)$ in (3.3) we obtain

$$K_1 > L_{00} := (A - 2 - K_2). \tag{3.7}$$

Now there are three cases. If $A \in (1 + \frac{K_2}{1+K_2}, 3 + K_2)$ then $M_{00} > 1$ and by (3.2) we have $m > m^*(n)$ and hence (2.12) is satisfied for all $K_1 > M_{00} > 1$. If $A = 3 + K_2$ then $L_{00} = M_{00} = 1$ and (2.12) is satisfied for all $K_1 > 1$. Finally if $A > 3 + K_2$ we have $L_{00} > 1 > M_{00}$ and (2.12) is satisfied for all $K_1 > L_{00} > 1$. This completes the proof of (i).

To prove (ii), first note that if $A \leqslant 3 + K_2$ then $m^*(n) \leqslant n(A-1) < m^0(n) + 1$ and so there is no integer $m \in (m^0(n), m^*(n))$ and nothing to prove. If $A > 3 + K_2$ then $m^*(n) > n(A-1)$ and for $m \in (n(A-1), m^*(n))$ the bound $\theta < 1$ is satisfied for all $K_1 > L_{nm} > 1$. Moreover we find that $G_{nm}(L_{nm}) < 0$, while the coefficient of the quadratic term is positive so (2.12) is satisfied for all $K_1 \in (L_{nm}, M^+_{nm})$, where M^+_{nm} is the largest root of $G_{nm}(K_1) = 0$.

In cases (iii) and (iv) we have $m > n(A-1)$ and $m \geqslant m^*(n)$. The bound $\theta < 1$ is satisfied for all $K_1 > 1$, while

$$G_{nm}(1) = K_2(2 + K_2)(m - n(A-1)) - K_2(A - 3 - K_2) \geqslant 0,$$

since $m \geqslant m^*(n)$. If and only if $K_1^* > 1$ and $G_{nm}(K_1^*) < 0$ where $G'_{nm}(K_1^*) = 0$ there will exist a nonempty interval (M^-_{nm}, M^+_{nm}) such that $1 \leqslant M^-_{nm} < K_1^* < M^+_{nm}$, $G_{nm}(M^\pm_{nm}) = 0$ and (2.12) is satisfied for all $K_1 \in (M^-_{nm}, M^+_{nm})$. But

$$G'_{nm}(K_1) = 2(m - n(A-1))(K_1 + K_2) - ((A-1)(1 + K_2) - K_2)$$

implies that

$$K_1^* = -K_2 + \frac{(A-1)(1+K_2) - K_2}{2(m - n(A-1))},$$

and $K_1^* > 1$ if and only if

$$m < n(A-1) + \frac{1}{2}(A-1) - \frac{K_2}{2(1+K_2)}. \tag{3.8}$$

To establish (iii) note that $m = m^*(n)$ implies both (3.8) and $G_{nm}(1) = 0$, thus $L_{nm^*} = M^-_{nm^*} = 1 < M^+_{nm^*}$. Moreover $m > m^0(n)$ implies $m > n(A-1)$ so the quadratic term in $G_{nm}(K)$ has a positive coefficient, and the conditions of Theorem 2.2 are satisfied for all $K_1 \in (1, M^+_{nm^*})$.

To establish (iv) let $\alpha = m - n(A-1)$ and $\beta = (A-1)(1+K_2) - K_2$. The condition $A > 1 + \frac{K_2}{1+K_2}$ implies that $\beta > 0$ while $m > m^0(n)$ implies $m > n(A-1)$ and hence $\alpha > 0$. The condition (3.8) for $K_1^* > 1$ can be rewritten as $\alpha < \frac{\beta}{2(1+K_2)}$, and we also find that

$$G_{nm}(K_1^*) = -\frac{1}{\alpha}\left(\frac{\beta}{2} - \alpha(1+K_2)\right)^2 + K_2\big[(1+\alpha)(2+K_2) - (A-1)\big]. \tag{3.9}$$

Then for $\alpha \in (0, \frac{\beta}{2(1+K_2)}]$ we see that $G_{nm}(K_1^*)$ is a strictly monotonically increasing function of α with $G_{nm}(K_1^*) > 0$ when $\alpha = \frac{\beta}{2(1+K_2)}$. Moreover, $\lim_{\alpha\to 0} G_{nm}(K_1^*) = -\infty$ and also $G_{nm}(K_1^*) < 0$ when $\alpha = \alpha^* = \frac{A-3-K_2}{2+K_2}$ (that is when $m = m^*(n)$), since then $G_{nm}(1) = 0 > G_{nm}(K_1^*)$. It follows that there exists $\alpha^{**} \in \big(\max\{0, \alpha^*\}, \frac{\beta}{2(1+K_2)}\big)$ such that $G_{nm}(K_1^*) < 0$ and $K_1^* > 1$ for all $\alpha \in (0, \alpha^{**})$ and $G_{nm}(K_1^*) \geqslant 0$ and/or $K_1^* \leqslant 1$ when $\alpha \geqslant \alpha^{**}$. Part (iv) follows on noting that $m = \alpha + n(A-1)$, so $m^{**}(n) = \alpha^{**} + n(A-1)$. The formula (3.4) for $m^{**}(n)$ follows from (3.9) on noting that $\alpha G_{nm}(K_1^*)$ is quadratic in α, and that α^{**} is given by the smaller root of $\alpha G_{nm}(K_1^*) = 0$.

Finally to prove (v), note that $m < m^0(n)$ implies $m \leqslant n(A-1) - 1$, in which case it is not possible to satisfy (3.1), and there is no unimodal solution satisfying the conditions of Theorem 2.2. The case of $m > m^{**}(n)$ was taken care of in the previous paragraph. □

In Theorem 3.1(i) we have shown that for $m = m^0(n)$, the smallest value of m for which a unimodal solution exists, the resulting solution exists for all K_1 sufficiently large. This holds

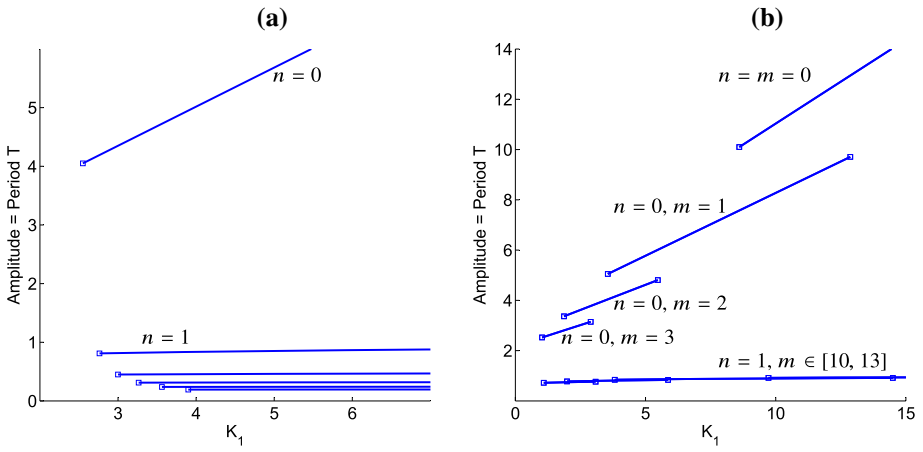

Fig. 6 **a** Periods of unimodal solutions for $m = m^0(n)$, $n = 0, 1, 2, 3, 4, 5$ (with decreasing period as n increases) satisfying Theorem 3.1(i), valid for all K_1 sufficiently large, with $a_2 = A = 5.05$. **b** Periods of legs of solutions satisfying the conditions of Theorems 2.2 and 3.1 for $a_2 = A = 11.1$, and $n = 0$ with $m = 0, 1, 2, 3$, and for $n = 1$ with $m = 10, 11, 12, 13$. In both cases $K_2 = 0.5$ and $a_1 = c = 1$

for each integer $n \geqslant 0$ and hence, as illustrated in Fig. 6a, we have found the far end of infinitely many solution branches. We note from (2.10) that the period T increases linearly with K_1 on the first ($n = 0$) branch, but that for $n > 0$ we have $\lim_{K_1 \to \infty} T = a_1/n$.

The remainder of this work is devoted to the extension and study of these bifurcation branches as well as their persistence for $\varepsilon > 0$. Most of the rest of each solution branch will be composed of legs of other unimodal solutions (with $m > n(A-1)$) and of bimodal solutions. Theorem 3.1(ii)–(iv) identifies the parts of the solution branch which are composed of unimodal solutions. This is illustrated in Fig. 6b.

From (2.10) we see that the unimodal solutions with the largest period occur on the branch $n = 0$. Let us consider this branch further. From Theorem 3.1(i) provided $A = a_2/a_1 > 1 + \frac{K_2}{1+K_2}$ there is a leg of unimodal solutions for $n = m = m^0(0) = 0$ for all $K_1 > \max\{L_{00}, M_{00}\}$. In that case Theorem 3.1 also ensures there will be legs of unimodal periodic solutions for each integer m between 0 and $m^{**}(0)$. Hence we require $m^{**}(0) > 1$ for there be a second leg of unimodal solutions with $n = 0$ and $m = 1$. Figure 7 shows the dependence of $m^{**}(0)$ on A and K_2, from which we see that we require the ratio $A = a_2/a_1 > 3$ for there to be a second, $m = 1$, leg of unimodal solutions for K_2 sufficiently small, while for $A > 5$ there is an $m = 1$ leg of unimodal solutions for all $K_2 \in (0, 1)$. Arbitrary large values of $m^{**}(0)$ are possible but require $A \gg 1$. We will explore the case $A \gg 1$ in Sect. 5. For other branches of solutions with $n > 0$, note that $m^0(n) \in (m^0(0) + n(A-1) - 1, m^0(0) + n(A-1)]$ and from (3.4) we have $m^{**}(n) = m^{**}(0) + n(A-1)$, and so for fixed A and K_2 essentially the same number of legs of unimodal solutions appear for each value of n, but the corresponding values of m are shifted by $n(A-1)$.

To show for a given value of n that the legs for different values of m form part of a connected branch of solutions we need to join them up, which we will do using bimodal periodic solutions of type I and II, and multi-modal solutions. First we note that if there is a continuous branch for fixed n then for A sufficiently large it must have fold bifurcations. To see this consider $m > m^0(n)$ in which case the coefficient of the quadratic term in (2.15) is positive, while by (3.3)

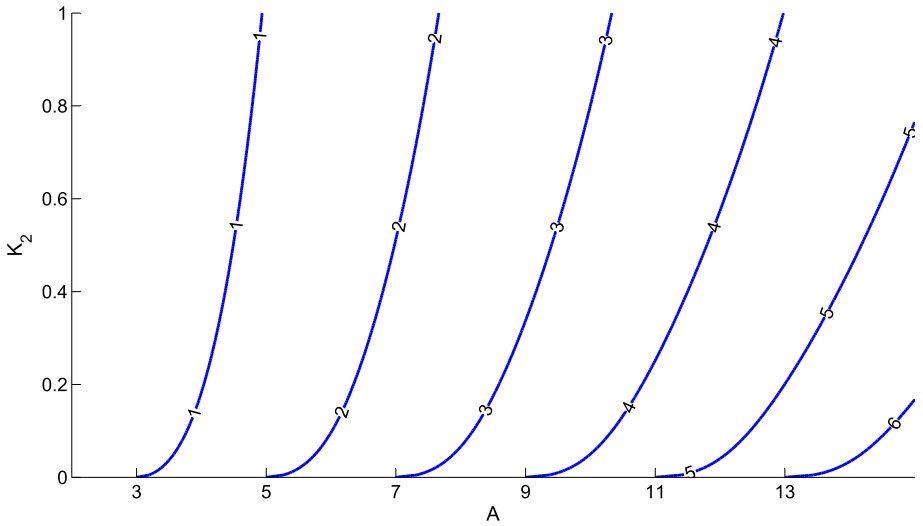

Fig. 7 Dependence of $m^{**}(n)$ given by (3.4) on $A = a_2/a_1$ and K_2 for the principal $n = 0$ branch. $m^{**}(0) > k$ to the right of each curve labelled k, and Theorem 3.1 then ensures there is a unimodal solution defined on an interval of K_1 values for $n = 0$ and each integer $m = 0, 1, \ldots, k$

$$G_{nm}(L_{nm-1}) = K_2(A-1)\left[2 + K_2 - \frac{A-2}{m - n(A-1)}\right].$$

Hence $G_{nm}(L_{nm-1}) < 0$ if $m < m^*(n) + \frac{1+K_2}{2+K_2}$. But since, M^+_{nm} is the largest zero of G_{nm} this implies that $L_{nm-1} < M^+_{nm}$. By (3.3) we also have $L_{nm} < L_{nm-1}$. Thus in the case of legs for $m = m^0(n), \ldots, M$ with $M < m^*(n) + \frac{1+K_2}{2+K_2}$ we have that $L_{nm-1} \in (L_{nm}, M^+_{nm})$ for $m = m^0(n) + 1, \ldots, M$. This implies that the K_1 values of legs for adjacent values of m overlap, just as illustrated in Fig. 6b. Hence if the legs form part of a continuous branch, the branch must have folds, as seen in Fig. 5. As Fig. 5 suggests, these will not be smooth fold bifurcations in the classical sense, but we will see in Sect. 4 that they are the $\varepsilon \to 0$ singular limit of smooth fold bifurcations of periodic orbits, and so we will refer to them as fold bifurcations anyway. We will see that these singular fold bifurcations typically occur at $K_1 = M^+_{nm}$ and $K_1 = L_{nm}$. To show this we need the following lemma which determines the sign of the denominator of (2.18), (2.19) and (2.25).

Lemma 3.2 *Let*

$$s(K_1) := 1 - m(K_1 - 1) + n(1 + K_1 + K_2). \tag{3.10}$$

If $m \in (m^0(n), m^*(n) + \frac{1+K_2}{2+K_2})$ *then* $s(L_{nm-1}) < 0$. *Moreover, if* $n = 0$ *or if* $n > 0$ *and* $A \geqslant 2 - 1/n$ *then* $s(K_1) < 0$ *for all* $K_1 \geqslant L_{nm-1}$. *Finally, if* $m > m^*(n) + \frac{1+K_2}{2+K_2}$ *then* $s(L_{nm-1}) > 0$.

Proof First note that from (3.3)

$$s(L_{nm-1}) = \frac{m\big[2 - A + (2+K_2)(m - n(A-1)\big]}{m - n(A-1)}.$$

Now $m > m^0(n)$ implies that $m - n(A-1) > 0$, while $m < m^*(n) + \frac{1+K_2}{2+K_2}$ implies $m - n(A-1) < (A-2)/(2+K_2)$ and hence $[2 - A + (2+K_2)(m - n(A-1)] < 0$ which shows

that $s(L_{nm-1}) < 0$. If $s(K_1)$ is a nonincreasing function of K_1, then it follows that $s(K_1) < 0$ for all $K_1 \geqslant L_{nm-1}$. But this is trivially true if $m \geqslant n$, which is always the case when $n = 0$, since $m \in \mathbb{N}_0$. For $n > 0$, provided $A \geqslant 2-1/n$, we have $m \geqslant m^0(n)+1 > n(A-1) \geqslant n-1$ and hence $m \geqslant n$. Finally $m > m^*(n) + \frac{1+K_2}{2+K_2}$ implies $[2 - A + (2+K_2)(m - n(A-1)] > 0$ which shows that $s(L_{nm-1}) > 0$. □

The following theorem establishes the existence of a fold bifurcation of periodic singular solutions at $K_1 = M^+_{nm}$. As noted before Lemma 3.2, this will not be a smooth bifurcation, but rather a leg of unimodal solutions and a leg of type I bimodal solutions will both exist for $K_1 \in (M^+_{nm} - \delta, M^+_{nm})$ and these solutions will coincide in the limit as $K_1 \to M^+_{nm}$. By coincide, we mean that the limiting profiles and periods of both solutions will be identical.

Theorem 3.3 *Let* $A = a_2/a_1 > 1$, $K_2 \in (0, 1)$, $n \in \mathbb{N}_0$ *and* $m^\dagger(n) = m^*(n) + \min\left\{\frac{1+K_2}{2+K_2}, 1 - \frac{A-1}{(2+K_2)(3+K_2)}\right\}$. *If* $m \in (n(A-1), m^\dagger(n))$ *then there exists* $\delta > 0$ *such that for* $K_1 \in (M^+_{nm} - \delta, M^+_{nm})$ *there is*

(a) *a leg of unimodal solutions satisfying the conditions of Theorem 2.2*
(b) *a leg of type I bimodal solutions satisfying the conditions of Theorem 2.3*

and these solutions coincide at $K_1 = M^+_{nm}$.

Proof Theorem 3.1 gives the existence of a leg of unimodal solutions for $K_1 \in (L_{nm}, M^+_{nm})$ or $K_1 \in (M^-_{nm}, M^+_{nm})$ when $m \in (n(A-1), m^*(n) + \frac{1+K_2}{2+K_2})$. Next we show that if there exists a leg of type I bimodal solutions for $K_1 \in (M^+_{nm} - \delta, M^+_{nm})$ then the unimodal and type I bimodal solutions must coincide in the limit as $K_1 \to M^+_{nm}$. To see this, compare the profile of the type I bimodal solution in (2.16) with the profile of the unimodal solution in Eqs. (2.2), (2.3). Since $G_{nm}(M^+_{nm}) = 0$, by (2.19) the bimodal solution must satisfy $\lim_{K_1 \to M^+_{nm}} T_2 = 0$. But when $T_2 = 0$ the bimodal profile corresponds to the unimodal profile. Elementary algebra then shows that the period T of the unimodal solution given by (2.10) equals the period T given by (2.18) for the bimodal profile when $G_{nm}(K_1) = 0$.

Finally we confirm the existence of the type I bimodal solution for $K_1 \in (M^+_{nm} - \delta, M^+_{nm})$ by verifying the conditions of Theorem 2.3. Since $G_{nm}(M^+_{nm}) = 0$, when $K_1 = M^+_{nm}$ by (2.19) we have $T_2 = 0$, and $T_1 = T$, where the value of T is given by (2.18) or (2.10). Now from (2.20)

$$\theta = \frac{a_2 - a_1 - mT}{T} = \frac{K_2}{K_1 + K_2 - 1} \in (0, 1),$$

using (2.11), (2.12) and the definition of M^+_{nm}. Thus the bounds (2.21) are trivially satisfied when $K_1 = M^+_{nm}$. The bound $\theta < 1 - 1/K_1$ also holds provided $K_2 < (K_1 - 1)^2$, in particular whenever $M^+_{nm} > 2$, but $M^+_{nm} > L_{nm-1}$ and $m < m^*(n) + 1 - \frac{A-1}{(2+K_2)(3+K_2)}$ implies that $L_{nm-1} > 2$.

Thus all the conditions for the existence of a type I unimodal solution from Theorem 2.3 are satisfied when $K_1 = M^+_{nm}$, and by continuity on an interval containing this point, except possibly for the condition $T_2 > 0$. But $T_2 = a_1 G_{nm}(K_1)/s(K_1)$ by (2.19). Now, noting that $G_{nm}(K_1) < 0$ for $K_1 \in (M^-_{nm}, M^+_{nm})$, and $G_{nm}(K_1) > 0$ for $K_1 > M^+_{nm}$, provided $s(M^+_{nm}) \neq 0$, the conditions of Theorem 2.3 must be satisfied on some interval $(M^+_{nm} - \delta, M^+_{nm})$ or $(M^+_{nm}, M^+_{nm} + \delta)$ by continuity of $s(K_1)$. But, by Lemma 3.2 we have $s(K_1) < 0$ for all $K_1 > L_{nm-1}$, and since $L_{nm-1} < M^+_{nm}$ it follows that for $\delta > 0$ sufficiently small that $s(K_1) < 0$ for $K_1 \in (M^+_{nm} - \delta, M^+_{nm} + \delta)$. Thus there is a unimodal solution for $K_1 \in (L_{nm}, M^+_{nm})$ and a bimodal solution on an interval $(M^+_{nm} - \delta, M^+_{nm})$ which coincide at a fold bifurcation at $K_1 = M^+_{nm}$. □

For values of m outside the range for which Theorem 3.3 is valid, it can still be possible to obtain type I bimodal and unimodal solutions which coincide at $K_1 = M_{nm}^+$ without a fold bifurcation. An example of this will be seen later in Fig. 20. We will not determine here the size of $\delta > 0$ such that Theorem 3.3 applies. However, we note that since the theorem guarantees the existence of the unimodal and type I bimodal solutions on some interval, it is a straightforward task to check the conditions of Theorems 2.2 and 2.3 to determine the interval on which each solution exists, and this is what we will do in later examples.

Since the proof of Theorem 3.3 is purely algebraic, it is interesting to consider the bifurcation from a dynamical viewpoint. For the leg of unimodal solutions θ approaches its lower bound in (2.12) as K_1 approaches M_{nm}^+ . Indeed, since $M_{nm}^{\pm}$ are the zeros of G defined by (2.15), it follows that $\theta \to K_2/(K_1+K_2-1)$ as $K_1 \to M_{nm}^{\pm}$ for all of the unimodal solutions identified in Theorem 3.1. At $K_1 = M_{nm}^{\pm}$ we have $F(5j+3) = 0$ in the proof of Theorem 2.2. The condition $F(5j+3) < 0$ in that proof ensures that F remains negative while $u(\mu_2(\eta))$, the value of u at the second delay, decreases from its maximum value $(-a_1 + (n+1)T)/c$ to its minimum value $(-a_1 + nT)/c$. If $F(\eta) = 0$ for some $\eta \in (5j+2, 5j+3)$ then the solution would reenter J^* and we would expect another interval on which $F(\eta) = 0$. This is exactly what happens in the bifurcation to the type I bimodal solution in Theorem 3.3. For the type I bimodal solution which exists for $K_1 < M_{nm}^+$, from the proof of Theorem 2.3 we see that for $\eta \in (10j+4, 10j+5)$ the solution at the second delay, $u(\mu_2)$ decreases from its maximum value $(-a_1+(n+1)T)/c$ to $(-a_1+nT+(1-s_{14})(1-\theta)T_1)/c$ with $F(\eta) < 0$, but $F(\eta) \to 0$ as $\eta \to 10j+5$. For $\eta \in (10j+5, 10j+6)$ we have $\eta \in J^*$, $F(\eta) = 0$ and $u(\mu_2)$ further decreases to its minimum value $(-a_1 + nT)/c$. However as K_1 approaches M_{nm}^+ we have $G_{nm}(K_1) \to 0$, and hence $T_2 \to 0$ and $s_{14} \to 1$, so $(-a_1+nT+(1-s_{14})(1-\theta)T_1)/c$ is no longer larger than $(-a_1+nT)/c$ and F does not become zero before $u(\mu_2)$ reaches its global minimum. Hence the second interval of J^* for $\eta \in (10j+5, 10j+6)$ collapses, and as s_{11} and s_{12} both tend to 1, we find that five of the intervals of the parametrisation of the type II bimodal solution become trivial, and the remaining parts correspond to the unimodal solution. Thus at the bifurcation between the unimodal solution and the type I bimodal solution θ hits its lower bound for the unimodal solution, and $T_2 \to 0$ for the bimodal solution. It will be interesting to investigate below what other bifurcations arise as other conditions in the theorems of Sect. 2 are violated.

Now consider the case of $K_1 = L_{nm-1}$ at the left end of the interval of unimodal solutions for $K_1 \in (L_{nm-1}, M_{nm-1}^+)$. We show there is a fold bifurcation here and the solution transforms from unimodal to a type II bimodal solution. By the definition of L_{nm} for $K_1 > L_{nm-1}$ the unimodal solution satisfies $a_2 - a_1 = (m-1+\theta)T$ with $\theta \in (0,1)$ but as $K_1 \to L_{nm-1}$ we have $\theta \to 1$. But if θ were equal to 1, the difference $a_2 - a_1$ between the two delayed times would be exactly m periods. Perhaps not surprisingly, as Theorem 3.4 shows, this can result in a (type II) bimodal solution with the value of m increased by 1.

Theorem 3.4 *Let $A = a_2/a_1 > 1$, $K_2 \in (0,1)$ and $n \in \mathbb{N}_0$.*

(i) *If $p \in [m^0(n)+1, m^*(n) + \frac{1+K_2}{2+K_2})$ then there exists $\delta > 0$ such that for $K_1 \in (L_{np-1}, L_{np-1}+\delta)$ there is*
(a) *a leg of unimodal solutions satisfying the conditions of Theorem 2.2 with $m = p-1$,*
(b) *a leg of type II bimodal solutions satisfying the conditions of Theorem 2.3 with $m = p$ and these solutions coincide at $K_1 = L_{np-1}$.*

(ii) *If $p \in (m^*(n) + \frac{1+K_2}{2+K_2}, m^*(n)+1]$ then there exists $\delta > 0$ such that*
(a) *for $K_1 \in (L_{np-1}, L_{np-1}+\delta)$ there is a leg of unimodal solutions satisfying the conditions of Theorem 2.2 with $m = p-1$,*

(b) *for* $K_1 \in (L_{np-1} - \delta, L_{np-1})$ *there is a leg of type II bimodal solutions satisfying the conditions of Theorem 2.3 with* $m = p$ *and these solutions coincide at* $K_1 = L_{np-1}$.

(iii) *If* $p \in \left(m^*(n)+1, \min\left(m^{**}(n)+1, (n+\frac{1}{2})(A-1)\right)\right)$ *then* $1-K_2 < L_{np-1} < 1 < M^-_{np-1} < M^+_{np-1}$ *and there exists* $\delta > 0$ *such that*

(a) *for* $K_1 \in (M^-_{np-1}, M^+_{np-1})$ *there is a leg of unimodal solutions satisfying the conditions of Theorem 2.2 with* $m = p-1$,

(b) *for* $K_1 \in (L_{np-1}-\delta, L_{np-1})$ *there is a leg of type II bimodal solutions satisfying the conditions of Theorem 2.3 with* $m = p$ *and these solutions exist on disjoint parameter intervals.*

Proof Theorem 3.1 gives the existence of a leg of unimodal solutions with $m = p-1$ for $K_1 \in (L_{np-1}, +\infty)$ when $p = m^0(n)+1$, for $K_1 \in (L_{np-1}, M^+_{np-1})$ when $p \in (m^0(n)+1, m^*(n)+1]$, and for $K_1 \in (M^-_{np-1}, M^+_{np-1})$ when $p \in [m^*(n)+1, m^{**}(n)+1)$.

To prove (i) and (ii), next we show that if there exists a leg of type II bimodal solutions with $m = p$ for $K_1 \in (L_{np-1} - \delta, L_{np-1})$ or $K_1 \in (L_{np-1}, L_{np-1} + \delta)$ then the unimodal and type II bimodal solutions must coincide in the limit as $K_1 \to L_{np-1}$. To see this, compare the profile of the type II bimodal solution in (2.17) with the profile of the unimodal solution in Eqs. (2.2), (2.3). The two solutions will coincide in the limit as $K_1 \to L_{np-1}$ if both the unimodal and type II bimodal solution have the same limiting period T and for the type II bimodal solution $\theta \to 0$ as $K_1 \to L_{np-1}$. But it is simple to check that the value of T given by (2.18) for the type II bimodal solution with $m = p$ agrees with that given by (2.10) for the unimodal solution with $m = p-1$. The rest of this proof concerns the existence and properties of the type II bimodal solution with $m = p$, so we can use m and p interchangeably. To show that $\theta \to 0$ as $K_1 \to L_{np-1}$ for the type II bimodal solution with $m = p$, note that by (2.18)

$$a_2 - a_1 - mT = a_1\left(A - 1 - \frac{mT}{a_1}\right) = \frac{a_1}{s(K_1)}\big[A - 1 - (m - n(A-1))(1 + K_1 + K_2)\big],$$

and from (3.3) we have

$$(L_{nm-1} + K_2 + 1)(m - n(A-1)) = A - 1. \tag{3.11}$$

Now, $s(L_{np-1}) \neq 0$ by Lemma 3.2, since $p \neq m^*(n) + \frac{1+K_2}{2+K_2}$. Hence

$$\lim_{K_1 \to L_{np-1}} \theta = \lim_{K_1 \to L_{np-1}} \frac{1}{T_2}(a_2 - a_1 - mT) = 0,$$

as required, provided $T_2 > 0$.

To derive expressions for T_1 and T_2 when $K_1 = L_{nm-1}$, using (2.25) and (3.11)

$$\begin{aligned} T_2 &= \frac{a_1}{s(L_{nm-1})} H_{nm}(L_{nm-1}) \\ &= \frac{a_1}{s(L_{nm-1})}\Big[(A-1)(K_1 + 2K_2 - 1) - K_1\big[(A-1)(1+K_2) - K_2\big] \\ &\qquad + K_2(1+K_2) + (A-1)(1-K_2)\Big] \\ &= \frac{a_1 K_2}{s(L_{nm-1})}\Big[(A-1)(1-K_1) + (1 + K_1 + K_2)\Big] = K_2 T. \end{aligned}$$

Thus $T_2 = K_2 T$ and $T_1 = (1-K_2)T$ when $K_1 = L_{nm-1}$. Since $K_2 \in (0,1)$ this implies that $T_1 > 0$ and $T_2 > 0$ in the limit as $K_1 \to L_{np-1}$, which establishes that the unimodal solution and type II bimodal solution have the same limiting profiles as $K_1 \to L_{np-1}$.

To prove (i) and (ii), it remains to verify the conditions of Theorem 2.4 to confirm the existence of the type II bimodal solution. First note that since $T_1 > 0$ and $T_2 > 0$ when $K_1 = L_{nm-1}$, and $s(L_{nm-1}) \neq 0$ there exists $\delta > 0$ such that T_1 and T_2 defined by (2.18), (2.25) vary continuously and are strictly positive for $K_1 \in (L_{nm-1} - \delta, L_{nm-1} + \delta)$. Now consider the condition $\theta > 0$. From above

$$\theta = \frac{a_1}{T_2}\frac{1}{s(K_1)}\big[A - 1 - (m - n(A-1))(1 + K_1 + K_2)\big].$$

Under (i) we have $s(L_{nm-1}) < 0$ and hence $s(K_1) < 0$ for $K_1 \in (L_{nm-1}, L_{nm-1} + \delta)$ for δ sufficiently small. Also by (3.11) for $K_1 > L_{nm-1}$ we have $A - 1 - (m - n(A-1))(1 + K_1 + K_2) < 0$. Hence $\theta > 0$ for $K_1 \in (L_{nm-1}, L_{nm-1} + \delta)$. Similarly under (ii) we have $s(L_{nm-1}) > 0$ and hence $s(K_1) > 0$ for $K_1 \in (L_{nm-1} - \delta, L_{nm-1})$ for δ sufficiently small, and by (3.11) we have $A - 1 - (m - n(A-1))(1 + K_1 + K_2) > 0$ for $K_1 > L_{nm-1}$. Thus under (ii) $\theta > 0$ for $K_1 \in (L_{nm-1} - \delta, L_{nm-1})$. Moreover since $\theta \to 0$ as $K_1 \to L_{nm-1}$ in both cases, for $\delta > 0$ sufficiently small we also have $\theta < 1$.

Next we show that the condition $\theta < \frac{T_1}{T_2} + 1 - \frac{1}{K_2}$ holds. Since $s(K_1)\big[A - 1 - (m - n(A-1))(1 + K_1 + K_2)\big] > 0$ for $K_1 \in (L_{nm-1} - \delta, L_{nm-1})$ under (i) and for $K_1 \in (L_{nm-1}, L_{nm-1} + \delta)$ under (ii), in both cases we have

$$\begin{aligned}
0 &< \frac{a_1}{K_2 s(K_1)}(K_1 + K_2 - 1)\big[(A-1) - (m - n(A-1))(1 + K_1 + K_2)\big] \\
&= \frac{m+1}{s(K_1)}\big[a_1(1 + K_1 + K_2) + (a_2 - a_1)(1 - K_1)\big] - (a_2 - a_1) - \frac{a_1 H_{nm}(K_1)}{K_2 s(K_1)} \\
&= (m+1)T - (a_2 - a_1) - \frac{1}{K_2}T_2 \\
&= T - \theta T_2 - \frac{1}{K_2}T_2, \quad \text{since } \theta T_2 = a_2 - a_1 - mT.
\end{aligned}$$

Hence $\theta T_2 < T_1 + T_2 - \frac{1}{K_2}T_2$, and since $T_2 > 0$ we have $\theta < \frac{T_1}{T_2} + 1 - \frac{1}{K_2}$ as required.

It remains only to establish (2.28) or (2.29). But for $p < m^*(n) + 1$, since $L_{np-1} > 1$ by Theorem 3.1, for $\delta > 0$ sufficiently small $K_1 > 1$ for all $K_1 \in (L_{np-1} - \delta, L_{np-1} + \delta)$, and so only (2.28) is required. But the right-hand side of (2.28) is strictly positive since $K_1 > 1 > K_2 > 0$, while from above $\theta \to 0$ as $K_1 \to L_{nm-1}$ so this inequality also holds for $\delta > 0$ sufficiently small. On the other hand if $p = m^*(n) + 1$ then $L_{np-1} = L_{nm^*} = 1$ and we need to verify (2.29) for $K_1 \in (L_{np-1} - \delta, L_{np-1}) = (1 - \delta, 1)$. But both expressions on the right-hand side of (2.29) are strictly positive for all K_1 sufficiently close to 1, while we already showed that $\lim_{K_1 \to L_{np-1}} \theta = 0$ and so (2.29) is satisfied for $K_1 \in (1 - \delta, 1)$. This establishes (i) and (ii).

To prove (iii) it remains only to establish the existence of the type II bimodal solution in that case, but this is similar to above, where we note that $p < (n + \frac{1}{2})(A-1)$ implies $L_{np-1} > 1 - K_2$ and choosing δ sufficiently small so that $L_{np-1} - \delta > 1 - K_2$ ensures that $K_1 + K_2 > 1$ for all $K_1 \in (L_{np-1} - \delta, L_{np-1})$. This implies that the second term on the right-hand side of (2.29) is strictly positive, while the first expression tends to $(L_{np-1} + K_2 - 1)/(L_{np-1} K_2) > 0$ in the limit as $K_1 \to L_{np-1}$. Again, since $\lim_{K_1 \to L_{np-1}} \theta = 0$, for $\delta > 0$ sufficiently small equation (2.29) is satisfied for $K_1 \in (L_{np-1} - \delta, L_{np-1})$. □

Theorem 3.4(i) establishes the existence of a fold bifurcation when $K_1 = L_{np-1}$ for $p \in \big(m^0(n), m^*(n) + \frac{1+K_2}{2+K_2}\big)$. Interestingly, for $p \in (m^*(n) + \frac{1+K_2}{2+K_2}, m^*(n) + 1]$ the fold disappears, but the two legs of periodic solutions continue to exist and coincide at $K_1 = L_{np-1}$, but now the type II bimodal solution exists for $K_1 < L_{np-1}$ while the unimodal solution exists for

$K_1 > L_{np-1}$. Essentially, the fold bifurcation unfolds suggesting a cusp-like bifurcation of periodic orbits, which we will investigate in Sect. 5.

Theorem 3.4(iii) also reveals interesting behaviour. When $m = m^*(n)+1$, or equivalently,

$$A = 1 + \frac{m(2+K_2)}{1+n(2+K_2)} \tag{3.12}$$

we have $L_{nm-1} = L_{nm^*} = 1$. Noting that $m^*(n) + 1 < (n + 1/2)(A - 1)$, for $m \in (m^*(n) + 1, (n + 1/2)(A - 1))$, or equivalently for

$$A \in \left(1 + \frac{2m}{1+2n}, 1 + \frac{(2+K_2)m}{1+(2+K_2)n}\right),$$

we have $1 > L_{nm-1} > 1 - K_2$ and Theorem 3.4(iii) ensures the existence of type II bimodal solutions for $K_1 \in (L_{nm-1} - \delta, L_{nm-1})$ where $1 - K_2 < L_{nm-1} - \delta < K_1 < L_{nm-1} < 1$. In contrast the construction of the unimodal and type I bimodal solutions in Theorems 2.2 and 2.3 requires $K_1 > 1$ for those solutions to exist.

Dynamically, we see in the proof of Theorem 3.4 that for both the unimodal and type II bimodal solution we have $T \to (a_2 - a_1)/m$ as $K_1 \to L_{nm-1}$. For the unimodal solution $(a_2 - a_1) = (m - 1 + \theta)T < mT$ and $\theta \to 1$ as $K_1 \to L_{nm-1}$, while for the type II bimodal solution $(a_2 - a_1) = mT + \theta T_2 > mT$ and $\theta \to 0$ as $K_1 \to L_{nm-1}$. Whether or not there is a (non-smooth) fold bifurcation at $K_1 = L_{nm-1}$ depends on whether m is greater or smaller than $m^*(n) + (1 + K_2)/(2 + K_2)$. That the value of m increases close to $K_1 = L_{nm-1}$ was already observed numerically for $\varepsilon > 0$ in [19].

Theorem 2.2 identified upper and lower bounds on θ for a unimodal solution to exist. In Theorems 3.3 and 3.4 we have shown bifurcations to type I or type II bimodal solutions when one of these bounds is violated. In later sections we will investigate the solutions that can arise when the parameter bounds identified in Theorems 2.3 and 2.4 for type I and II bimodal solutions are violated.

4 Singularly Perturbed Solution Branches

We are interested in solutions of (1.2) when $0 < \varepsilon \ll 1$. However, so far we have only constructed $\varepsilon = 0$ singular solutions, in the sense of Definition 1.2. It would be desirable to prove that (1.2) has solutions close to the constructed singular solutions for all ε sufficiently small. Mallet-Paret and Nussbaum [31] proved that the sawtooth is indeed the limiting profile as $\varepsilon \to 0$ for the state-dependent DDE (1.3) which has only one delay. However, for the two delay problem (1.1), Theorems 3.3 and 3.4 lead us to expect fold bifurcations of periodic orbits. Indeed such bifurcations and resulting intervals of co-existing stable periodic solutions were already observed for $\varepsilon = \mathcal{O}(1)$ in [19]. 'Superstability' is central to the results of [31], and without further insight it is difficult to see how to modify the techniques of [31] to rigorously prove the persistence of the singular solutions for $\varepsilon > 0$ given that it is possible for (1.1) to have co-existing stable periodic orbits. Nevertheless, Mallet-Paret and Nussbaum have announced as yet unpublished results [32].

Given the analytical difficulties, in the current work we will instead use the algebraic results for $\varepsilon = 0$ from the previous sections to guide a numerical study of the periodic solutions and bifurcation structures for (1.1) for $1 \gg \varepsilon > 0$. From the numerical solutions we will see that over wide parameter ranges the singular solutions identified in the theorems of Sects. 2 and 3 are indeed the limits of the solutions of the DDE (1.1) as $\varepsilon \to 0$. Moreover

we will find that that (1.1) has fold bifurcations of periodic orbits at K_1 values which converge to $K_1 = L_{nm}$ and $K_1 = M_{nm^+}$ in the limit as $\varepsilon \to 0$.

For $\varepsilon > 0$ we compute bifurcation branches numerically using DDEBiftool [11]. DDEBiftool is a suite of MATLAB [33] routines for computing solution branches and bifurcations of DDEs using path following and branch switching techniques. Periodic orbits are found as the solution of a boundary value problem (BVP), using collocation techniques. The numerical analysis details are well described in [11] and elsewhere, so we will not repeat them here. We emphasise however, that periodic orbits are found by solving BVPs, and *not* by solving initial value problems. This allows unstable orbits to be found just as easily as stable ones. DDEBiftool can determine the stability of periodic orbits by computing their Floquet multipliers which also allows us to detect bifurcations. In [19] we already used DDEBiftool to investigate the dynamics of (1.1) in the non-singular case $\varepsilon = 1$.

We will mainly concentrate our attention on the principal branch of periodic solutions, which is the only one on which we found large amplitude stable solutions for $\varepsilon > 0$. By the principal branch, we mean the branch of periodic orbits which has the largest period among all the Hopf bifurcations, both at the bifurcation and in the limit as $K_1 \to \infty$. This usually also corresponds to the Hopf bifurcation with the smallest value of K_1, but due to the vagaries of the behaviour of the characteristic values in DDEs for ε very close to zero, it is sometimes possible for a shorter period orbit to bifurcate first. If that happens the orbit on the principal branch is initially unstable but we found numerically that it becomes stable in a torus bifurcation while its amplitude is still very small. In the current work we will not study small amplitude solutions or invariant tori (see [4] for a study of the invariant tori of (1.1), and [22] for a study of (1.3) close to the singular Hopf bifurcation). The principal branch will always correspond to the choice $n = 0$ for the singular solutions and hence $m^0 = 0$.

Throughout this work, the amplitude of a periodic orbit of period T is defined simply as the difference between the maximum and minimum values of $u(t)$ over the period. We will take $c = 1$ and $K_2 = 0.5$ in all our examples, and $a_1 = 1$, so $A = a_2/a_1 = a_2$.

Figure 8 illustrates the convergence of the principal solution branch as $\varepsilon \to 0$. For $A = 6$, the amplitudes of the periodic solutions on the branch are plotted against the bifurcation parameter K_1 for different values of $\varepsilon > 0$. Also shown are the amplitudes of the $\varepsilon = 0$ singular solutions following from the results of Sects. 2 and 3.

For $A = 6$ and $K_2 = 0.5$ with $n = m^0 = 0$, we have $m^* = 1$ and $m^{**} \approx 1.6$. Hence by Theorem 3.1 there are legs of unimodal singular solutions with $m = 0$ for $K_1 > L_{00} = 3.5$ and with $m = 1$ for $K_1 \in (M_{01}^-, M_{01}^+) = (1, 5)$. Theorems 3.3 and 3.4 ensure that there are legs of type I and type II bimodal solutions with $m = 1$ for K_1 between L_{00} and M_{01}^+. By verifying the conditions of Theorems 2.3 and 2.4 we find that the type I bimodal solutions exist for $K_1 \in (4.7122, 5)$ and the type II solutions for $K_1 \in (3.5, 4.5549)$.

Figure 8 shows that the branch converges over its entire length as $\varepsilon \to 0$, and on the intervals where singular solutions exist the amplitudes converge to those of the singular solutions. For $\varepsilon > 0$ the orbits have slightly smaller amplitude than the singular solutions, which is to be expected since the singular solutions are of sawtooth shape, while for $\varepsilon > 0$ the orbits are smooth, and some amplitude is lost in the "smoothing". Insets in Fig. 8 show solution profiles on the unstable middle leg of solutions for $K_1 = 4.4$, $K_2 = 0.5$, converging to a type II bimodal solution (also shown) as $\varepsilon \to 0$. Even for ε as large as 0.2 the bimodal sawtooth structure of the solution profile is very clearly seen. For larger ε the solution profiles are smoother, particularly near the local maxima, but the fold structure on the solution branch persists even when $\varepsilon = 1$.

Figure 8 is representative of the behaviour for other values of A. Not only do the singular solutions constructed as in Sect. 3 give the limiting amplitudes for the bifurcation branches

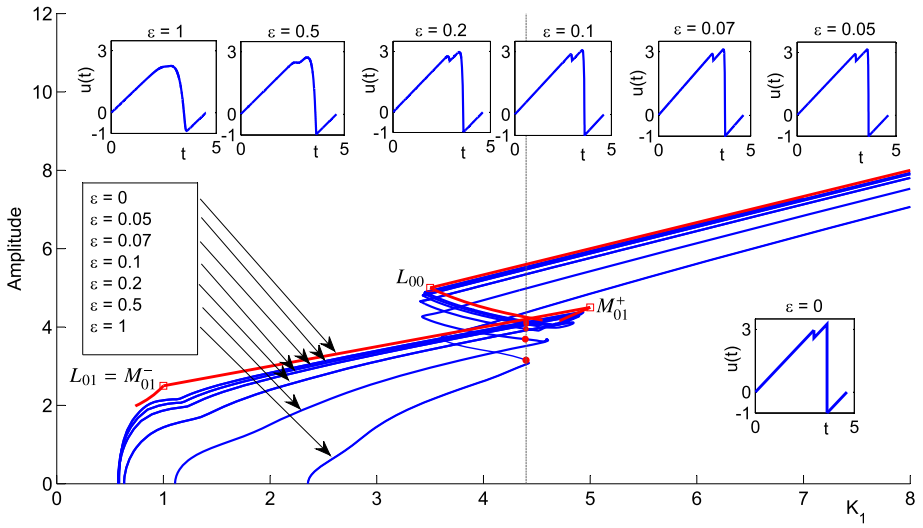

Fig. 8 Superimposed plots of the amplitude of the periodic solutions on the principal branch created from a Hopf bifurcation as K_1 is varied for different values of ε with $K_2 = 0.5$, $A = a_2 = 6$, $a_1 = c = 1$. The legs of $n = 0$ unimodal and type I and II bimodal singular $\varepsilon = 0$ solutions, are shown in *red*, and the singular fold bifurcations are labelled by L_{00} and M_{01}^{+}, using the notation of Sect. 3. The branches for $\varepsilon > 0$ are computed using DDEBiftool. For $K_1 = 4.4$ the profile of the $\varepsilon = 0$ type II singular solution on the middle leg is also shown, along with corresponding numerically found periodic orbit profiles for $\varepsilon > 0$ (Color figure online)

as $\varepsilon \to 0$, but the points L_{nm} and M_{nm}^{+} give the limiting locations of the fold bifurcations. Moreover, we will see in Sect. 5 that the singular solution theory is robust enough to show the location of codimension-two cusp-like bifurcations.

Figure 9 shows the bifurcation branch for $\varepsilon = 0.1$ plotted against the period, along with the $\varepsilon = 0$ singular solutions for the same values of the other parameters as Fig. 8. Profiles of periodic orbits for $\varepsilon = 0.1$ are also shown. Where the singular solutions exist their period is very close to that of the numerically computed $\varepsilon = 0.1$ solutions. The agreement in period is even better than the agreement in amplitude between the singular and $\varepsilon = 0.1$ solutions seen in Fig. 8. For $\varepsilon = 0.1$ the periodic solutions before the first fold and after the second fold are stable with an interval of bistability of periodic solutions between the two folds. Periodic solutions on the leg of the branch between the two folds are always unstable, and are bimodal for at least part of the leg. On the leg of unstable solutions in Fig. 9 we see two types of bimodal periodic solutions for $\varepsilon = 0.1$, where either the first or second local maximum after the solution minimum is higher (see insets with $K_1 = 4.8001$ and $K_1 = 4.1993$). Note the resemblance between the profiles of the $\varepsilon = 0.1$ solutions and the singular solutions shown in Figs. 3 and 4, which is not coincidental; the construction of the singular solutions in Sect. 2 was guided by preliminary numerical computations.

We see in Figs. 8 and 9 that the $\varepsilon > 0$ branches pass continuously through the gap in the singular solution branch. With $\varepsilon = 0.1$ there is a smooth transition between the two types of bimodal solutions along the unstable leg, whereas Fig. 5 suggests that there should be a gap between the intervals where these two types of solutions exist in the limit as $\varepsilon \to 0$. So we next investigate periodic solution profiles as $\varepsilon \to 0$ paying particular attention to the legs between the fold bifurcations where those gaps occur.

For $\varepsilon = 0.05$ we find periodic solutions with three local maxima per period (which we call trimodal solutions) on the unstable leg of the branch for an interval of K_1 values which falls

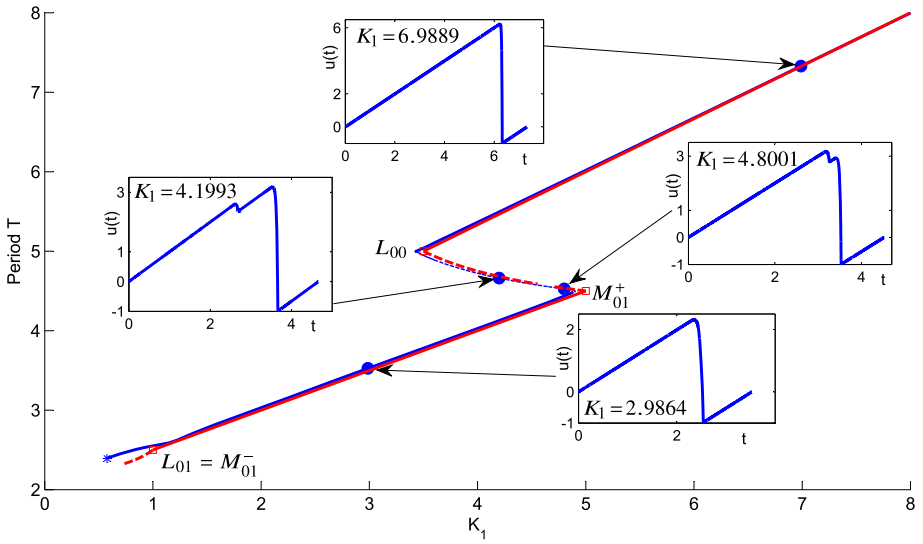

Fig. 9 Periods of orbits on the principal branch with $\varepsilon = 0.1$ (in *blue*), and the legs of $\varepsilon = 0$ singular unimodal and bimodal solutions (in *red*). Other parameters have the same values as in Fig. 8. Unimodal singular solutions exist with $m = 0$ for $K_1 > L_{00} = 3.5$, and with $m = 1$ for $K_1 \in (M_{01}^-, M_{01}^+)$ where $M_{01}^- = L_{01} = 1$ and $M_{01}^+ = 5$. Legs of bimodal solutions of type I exist for $K_1 \in (4.7122, 5)$ and of type II for $K_1 \in (3.5, 4.5549)$. *Insets* show solution profiles for $\varepsilon = 0.1$. For $\varepsilon = 0.1$ solutions are unstable between the folds, and stable on the upper and lower legs of the branch (Color figure online)

within the gap between the type I and type II bimodal singular solutions. Figure 10 shows the profiles of two of these trimodal periodic solutions. We note that both profiles are similar to bimodal solutions, but that in both cases the first local maxima of the bimodal solution has split into two local maxima. For parameter values close to where the type I bimodal solutions exist (including $K_1 = 4.659$) the first two local maxima of the solution resemble those of a type I bimodal solution (with the first local maxima after the global minima being the global maxima), while for parameter values close to the type II bimodal solutions (including $K_1 = 4.6294$) the first two local maxima of the solution resemble those of a type II bimodal solution (with the second local maxima after the global minima being the global maxima).

With $\varepsilon = 0.01$ on the unstable leg of the branch, Type I-like bimodal solutions occur in the approximate range $K_1 \in (4.6998, 4.9802)$. At $K_1 \approx 4.6998$ there is a transition to a trimodal solution, and trimodal solutions exist for $K_1 \in (4.6735, 4.6998)$. The numerically found trimodal solution for $K_1 = 4.6908$ is shown in Fig. 11a. Again we see (in the inset) that it is the first maximum of the solution which splits into two to form the trimodal solution. Around $K_1 \approx 4.673$ there is a brief interval of quadrimodal solutions, where the first maximum of the trimodal solution splits into two as shown in Fig. 11c. There is then another interval of trimodal solutions for $K_1 \in (4.5746, 4.673)$, with the solution for $K_1 = 4.6266$ shown in Fig. 11b. Finally for $K_1 < 4.5746$ the solutions are bimodal (and type II-like). Comparing the trimodal solutions in Figs. 10 and 11 we see that the trimodality is much more clearly defined for the smaller value of ε with the profiles in Fig. 11 much more 'sawtooth-like' than the smoother profiles seen in Fig. 10. Moreover, for both $\varepsilon = 0.05$ and $\varepsilon = 0.01$ the trimodal solution in the interval adjacent to the type I bimodal solutions has a larger first peak than second peak, just as the type I bimodal solutions do, and similarly for type II bimodal solutions and the trimodal solutions in the adjacent parameter interval the second peak is larger. This could lead us to define type I and type II trimodal solutions which could be found algebraically in the $\varepsilon = 0$

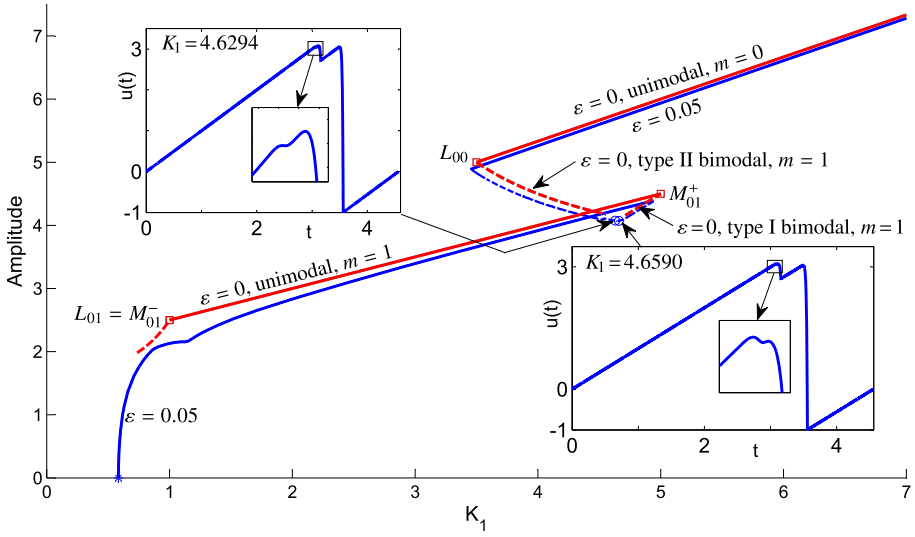

Fig. 10 Amplitude of $\varepsilon = 0.05$ and singular solutions, with the other parameters taking the same values as in Fig. 8. For $\varepsilon = 0.05$ periodic solutions with three local maxima per period (trimodal solutions) are found on a small interval for $K_1 \in (4.6294, 4.6668)$. Profiles of two of these trimodal periodic solutions with $K_1 = 4.6294$ and $K_1 = 4.6590$ are shown as *insets*

limit using our singular solution techniques. However each would involve about 15 intervals of parametrisation, which would be tedious beyond belief. Moreover, Fig. 11 suggests that the quadrimodal solutions also come in both types, and we suspect that as $\varepsilon \to 0$ there is a cascade of solutions with arbitrarily many maxima, and some form of self-similarity to the evolution of the periodic solution profile in the limit as $\varepsilon \to 0$. However all these multimodal solutions lie on the unstable leg of the branch, and we will not pursue their construction here.

Although we omit the algebraic construction of trimodal solutions, our construction of the bimodal solutions is sufficient to compare the bimodal to trimodal solution transition with the unimodal to bimodal transitions/bifurcations already studied algebraically in Sect. 3. The interval of K_1 values for which type I bimodal solutions exist was found by checking the conditions of Theorem 2.3. In all the examples shown above, and indeed in the other examples of type I bimodal solutions that occur later in this paper we only find two different behaviours which arise at the ends of these intervals. One case is when $K_1 = M^+_{nm}$ indicating a transition or bifurcation between a unimodal and type I bimodal solution as studied in Theorem 3.3 and the comments after that theorem. At the other end of the leg of type I bimodal solutions where the $\varepsilon > 0$ numerics indicate a transition to a trimodal solution, algebraically in all the examples shown here we find that the lower bound on θT_1 in (2.21) fails. From the proof of Theorem 3.3 we see that equality in this bound corresponds to $F(10j + 3) = 0$. This is similar to the transition from a unimodal to type I bimodal solution at $K_1 = M^+_{nm}$ as described after Theorem 3.3. Then we saw that the failure of the condition $F(5j + 3) < 0$ in the unimodal singular solution led to the creation of a second subinterval of J^* in the periodic orbit. In an analogous manner the failure of the condition $F(10j + 3) < 0$ in the type I bimodal singular solution can lead to a solution where J^* consists of three disjoint intervals per period and the resulting solution is trimodal.

The transition from type II bimodal to trimodal solutions also appears to be similar to the transition from unimodal to type II bimodal solutions. After Theorem 3.4 we noted that at the transition between unimodal and type II bimodal solutions at $K_1 = L_{nm-1}$ we have $\theta \to 1$

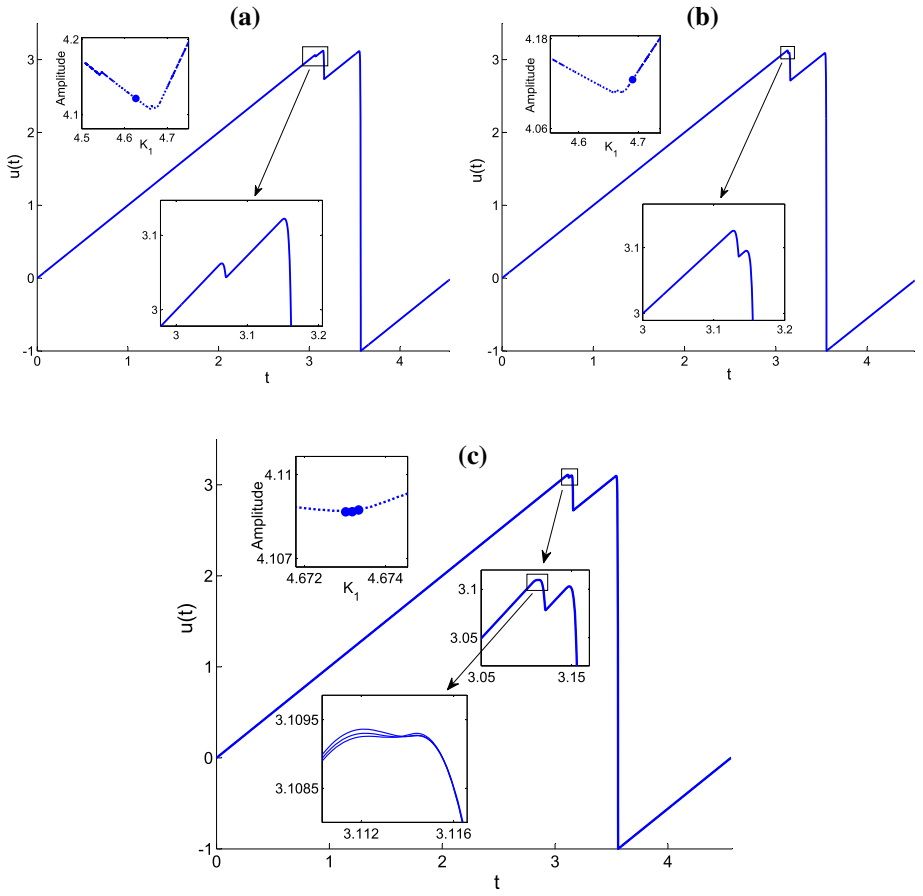

Fig. 11 For $\varepsilon = 0.01$ and the other parameters as in the preceding figures, trimodal periodic solutions are found for $K_1 \in (4.5747, 4.6999)$ and within this interval solutions are quadrimodal for $K_1 \in (4.6730, 4.6733)$. Shown are two example profiles of trimodal solutions **a** for $K_1 = 4.6908$, and **b** for $K_1 = 4.6266$, and **c** three quadrimodal solutions (plotted on the same axis)

for the unimodal solution and $\theta \to 0$ for the type II bimodal solution as $K_1 \to L_{nm-1}$. Checking the conditions of Theorem 2.4 we find that in all the examples above $\theta \to 0$ as $K_1 \to L_{nm-1}$ and $\theta \to 1$ at the other end of each leg of type II bimodal solutions. We would expect the solution to transition to a type II trimodal solution with $\theta = 0$ at this point.

5 Cusp-like Bifurcations

Here we investigate the cusp-like bifurcations, identified by Theorem 3.4, where fold bifurcations of singular solutions disappear when $m = m^*(n) + \frac{1+K_2}{2+K_2}$ and $K_1 = L_{nm-1}$, or equivalently when

$$A = 1 + \frac{1 + m(2 + K_2)}{1 + n(2 + K_2)}, \quad K_1 = L_{nm-1} = 1 + \frac{1 + n(2 + K_2)}{m - n}. \tag{5.1}$$

On the principal branch $n = 0$, so the cusps occur when $A = 2 + m(2 + K_2)$ and $L_{0m-1} = 1 + 1/m$. Taking $K_2 = 0.5$, the cusp-like bifurcations for the singular solutions occur when

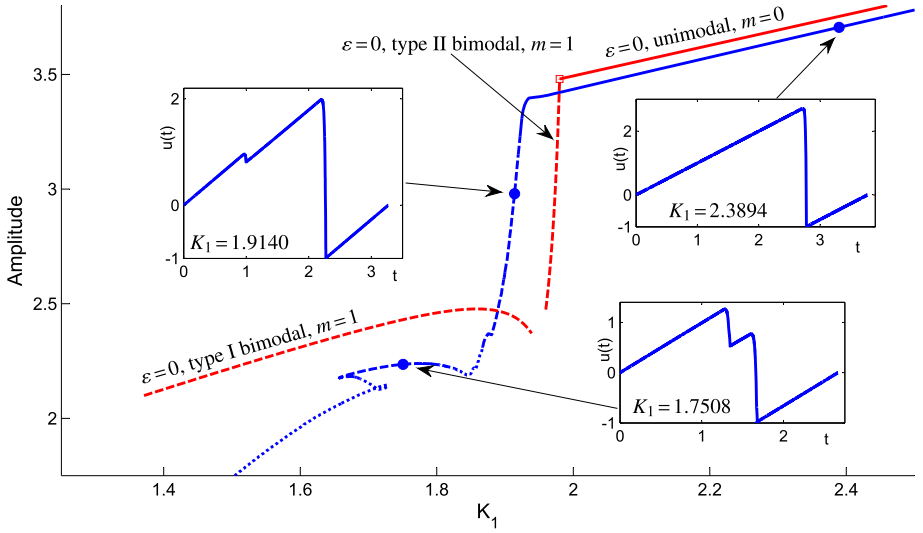

Fig. 12 Amplitude of Type I and II bimodal singular solutions with $m = 1$ and unimodal solutions with $m = 0$ for $A = 4.48$, $K_2 = 0.5$ and $n = 0$. Also shown is the numerically computed principal branch of periodic orbits for the same parameters except $\varepsilon = 0.02$. Unimodal, bimodal and multimodal periodic orbits occur on the *solid*, *dashed* or *dotted* parts of the bifurcation curve, respectively. *Insets* show profiles of stable numerically computed orbits with $\varepsilon = 0.02$ corresponding to unimodal, and type I and II bimodal solutions

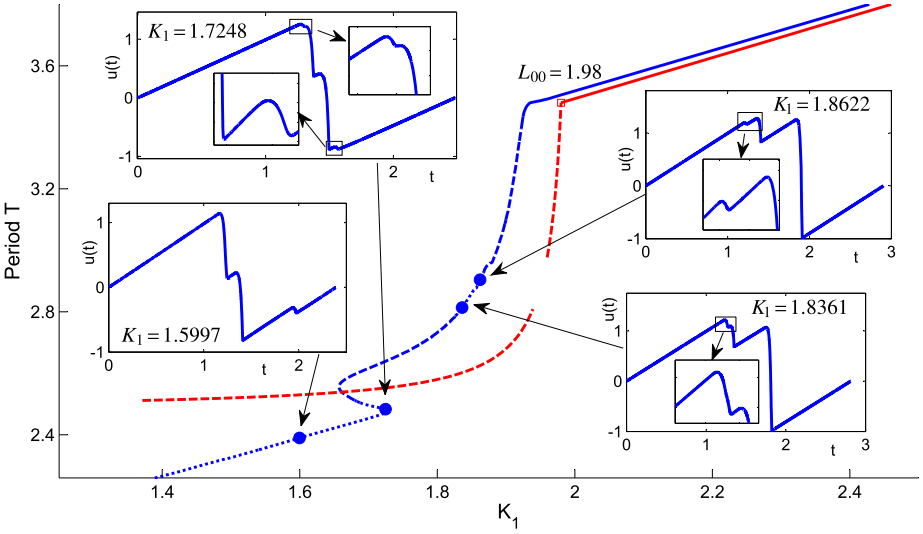

Fig. 13 Periods of $\varepsilon = 0$ singular solutions and the numerically computed $\varepsilon = 0.02$ solution branch for the same parameters as Fig. 12. *Insets* show profiles of numerically computed type I and II trimodal solutions for $K_1 = 1.8361$ and 1.8622, as well as examples of trimodal and quadrimodal solutions found earlier on the branch. All the *inset* solutions are unstable with a complex conjugate pair of unstable Floquet multipliers

$A = 4.5, 7, 9.5, \ldots$ and $L_{0m-1} = 2, 3/2, 4/3, \ldots$. Here we will investigate the first two such bifurcations both in the singular case with $\varepsilon = 0$, and numerically for $0 < \varepsilon \ll 1$.

Figures 12, 13, 14 and 15 illustrate the change in the dynamics near to $K_1 = L_{00}$ as A passes through 4.5. Amplitude and period plots of the unimodal and bimodal singular

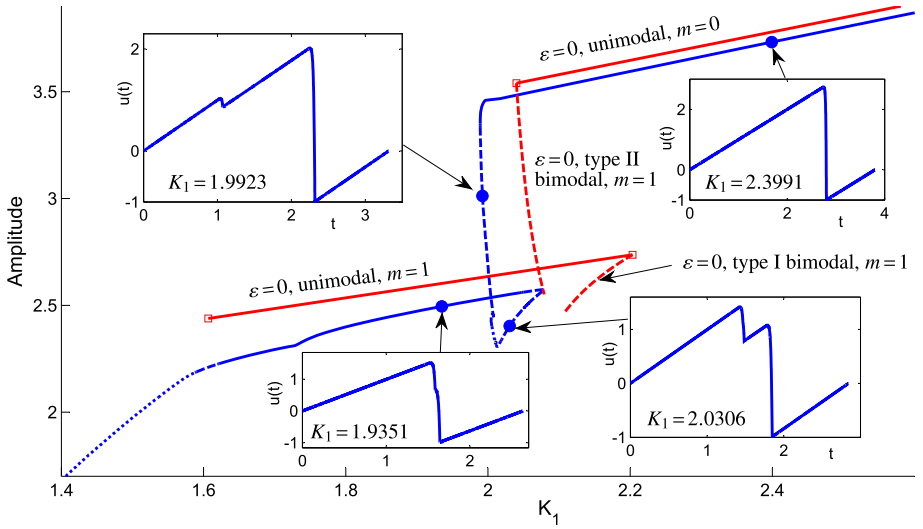

Fig. 14 Amplitudes of Type I and II bimodal singular solutions with $m = 1$ and unimodal solutions with $m = 0$ and $m = 1$ for $A = 4.54$, $K_2 = 0.5$ and $n = 0$. The numerically computed principal branch of periodic orbits with $\varepsilon = 0.02$ is also shown. *Insets* show profiles of stable numerically computed periodic orbits. The unimodal orbits with $K_1 = 1.9351$ and $K_1 = 2.3991$ are stable, while the other two orbits which correspond to type I and II bimodal solutions are unstable with one real unstable Floquet multiplier

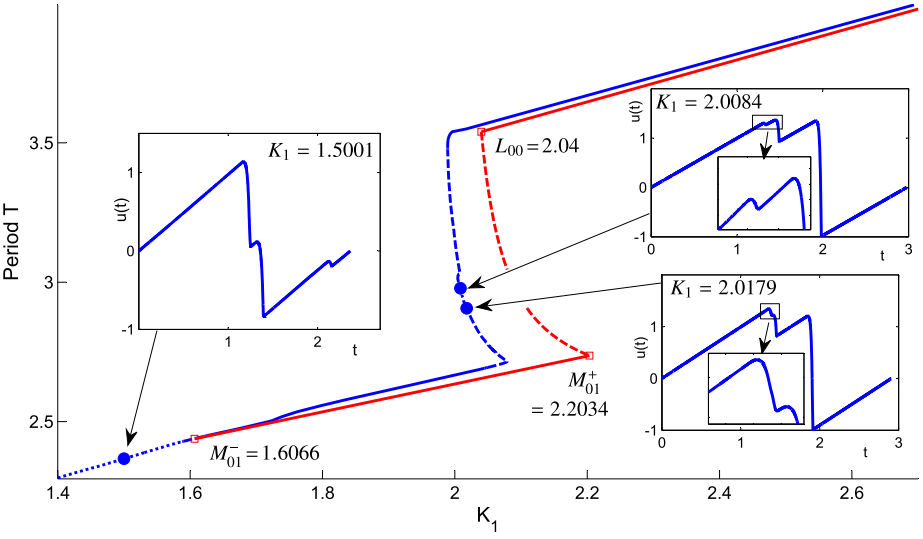

Fig. 15 Periods of $\varepsilon = 0$ singular solutions and the numerically computed $\varepsilon = 0.02$ solution branch for the same parameters as Fig. 14. *Insets* show profiles of trimodal solutions on the $\varepsilon = 0.02$ branch, which are all found to be unstable

solutions are shown for $A = 4.48$ and $A = 4.54$ along with the numerically computed principal branch of periodic solutions with $\varepsilon = 0.02$. By Theorem 3.4 we have a leg of unimodal singular solutions for $K_1 > L_{00} = A - 2 - K_2$ with period $T \to A - 1$ as $K_1 \to L_{00}$, and since $c = 1$, amplitude equal to the period. For $A = 4.48$ and $K_2 = 0.5$ this

gives $L_{00} = 1.98$ with the period and amplitude of the unimodal solutions tending to 3.48 as $K_1 \to L_{00}$. Moreover (3.2) implies $m^*(0) + \frac{1+K_1}{1+K_2} < 1$ and Theorem 3.4(ii) gives the existence of a leg of type II bimodal solutions for $K_1 < L_{00}$. We see from Figs. 12 and 13 that the solution branch for $\varepsilon = 0.02$ behaves similarly though the transition point is perturbed to $K_1 \approx 1.9221$ which is slightly less than $L_{00} = 1.98$.

For $A = 4.54$, $m^0(0) = 0$ and $m^*(0) + \frac{1+K_1}{1+K_2} > 1$, thus Theorem 3.4(i) gives the existence of a leg of type II bimodal solutions for $K_1 > L_{00}$, resulting in a fold bifurcation. Figures 14 and 15 show that the $\varepsilon = 0.02$ solution branch also has a fold bifurcation for $K_1 \approx 1.9892$ slightly less than $L_{00} = 2.04$, with the solution profile changing from unimodal to bimodal (see insets in Fig. 14 for $K_1 = 1.9351$ and $K_1 = 2.3991$). Similarly, for $A = 4.54$, Theorem 3.3 indicates a second fold bifurcation of singular solutions at $K_1 = M_{01}^+ = 2.2034$ where the solution profile also transitions between a unimodal and a type I bimodal solution, and Figs. 14 and 15 show that the numerically computed branch for $\varepsilon = 0.02$ has a similar bifurcation at $K_1 \approx 2.079$. Insets in Fig. 14 for $K_1 = 1.9923$ and $K_1 = 2.0306$ show the resulting unimodal and bimodal solutions each side of this fold. Trimodal solutions of both types are also observed on the $\varepsilon = 0.02$ branch for both $A = 4.48$ and $A = 4.54$ for parameters in the gap between the $m = 1$ bimodal type I and type II solutions, and these are illustrated in insets in Figs. 13 and 15.

One important aspect of this cusp-like bifurcation is that it has the potential to create stable bimodal and multimodal periodic solutions. In Sect. 4 all of the solutions with more than one local maxima per period were unstable occurring on the leg of the bifurcation branch between the fold bifurcations. The bimodal and trimodal solutions occurring between the fold bifurcations for $A = 4.54$ illustrated in Figs. 14 and 15 are also unstable. However before the cusp bifurcation with $A \lessapprox 4.5$ stable periodic solutions with more than one local maxima per period occur close to $K_1 = L_{00}$ on the principal branch. Figure 12 illustrates stable bimodal solutions for $\varepsilon = 0.02$ and $K_1 = 1.7508$ and $K_1 = 1.9140$ which correspond to $\varepsilon = 0$ type I and type II bimodal singular solutions. Interestingly the type I and II trimodal solutions for $A = 4.48$ and $K_1 = 1.8361$ and $K_1 = 1.8622$ illustrated in Fig. 13 are unstable, even though they are not between fold bifurcations. Both these periodic orbits have a pair of complex conjugate unstable Floquet multipliers, indicating a possible torus bifurcation.

The agreement between the singular solution legs and the $\varepsilon = 0.02$ branch is not as good for the smaller values of K_1 shown in Figs. 12 and 13 when $A = 4.48$. In particular for the singular solution there is a leg of type I bimodal solutions with $m = 1$ for $K_1 \in (M_{01}^-, M_{01}^+) \approx (1.3711, 1.9391)$, but for $\varepsilon = 0.02$ the corresponding bimodal solution only exists in the interval $K_1 \in (1.6571, 1.8259)$. To explain this note that the interval (M_{01}^-, M_{01}^+) is derived from the roots of a quadratic with parameters such that it is close to its double root and is thus very sensitive to the value of A; decreasing A to 4.41 causes this interval and the associated type I bimodal singular solutions to vanish. Computations with other values of A (not shown) suggest that for $\varepsilon = 0.02$ the fold bifurcation associated with the point $K_1 = L_{00}$ disappears at about $A = 4.52$, whereas this occurs at $A = 4.5$ for the singular solution, hence the $\varepsilon = 0.02$ solution branch for $A = 4.48$ is actually twice as far from its critical value as the singular solutions shown in the same figures, so it is not surprising that $\varepsilon = 0.02$ bimodal solution exists on a smaller interval.

Although, as expected, Figs. 12 and 13 do not display a fold bifurcation between the unimodal and bimodal solutions near $K_1 = L_{00}$ with $A = 4.48$, we note that two fold bifurcations are visible earlier on the branch in this case at $K_1 \approx 1.6571$ and $K_1 \approx 1.7282$. These folds are not associated with unimodal solutions but with bimodal and multimodal solutions. An inset for $K_1 = 1.7248$ in Fig. 13 shows a periodic solution with 4 local maxima per period close to one of these folds.

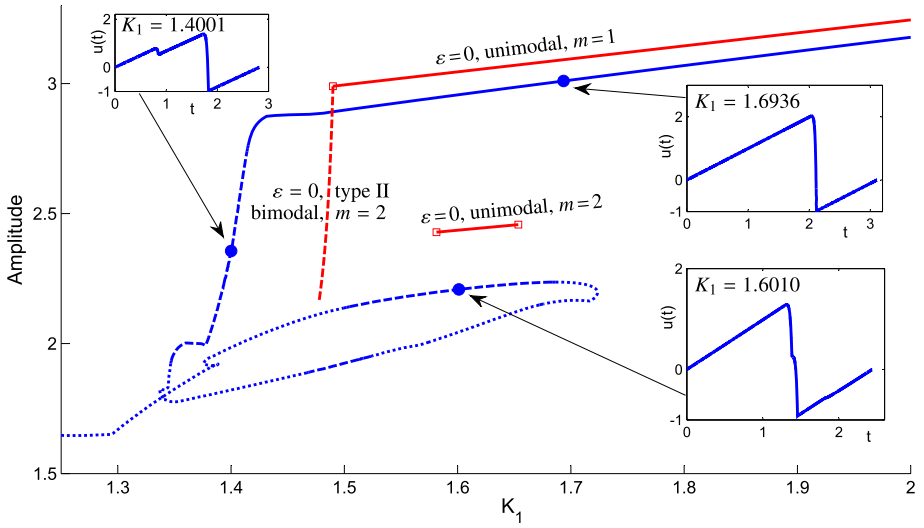

Fig. 16 Amplitudes of Type I and II bimodal singular solutions with $m = 2$ and unimodal solutions with $m = 1$ for $A = 6.98$, $K_2 = 0.5$ and $n = 0$. Also shown is the numerically computed principal branch of periodic orbits for the same parameters except $\varepsilon = 0.02$. Unimodal, bimodal and multimodal periodic orbits for $\varepsilon = 0.02$ occur on the *solid*, *dashed* or *dotted parts of the curve*, respectively. *Insets* with $K_1 = 1.6936$ and $K_1 = 1.4001$ show profiles of $\varepsilon = 0.02$ stable unimodal and type II bimodal periodic orbits. See text for discussion of the $K_1 = 1.601$ unstable bimodal solution

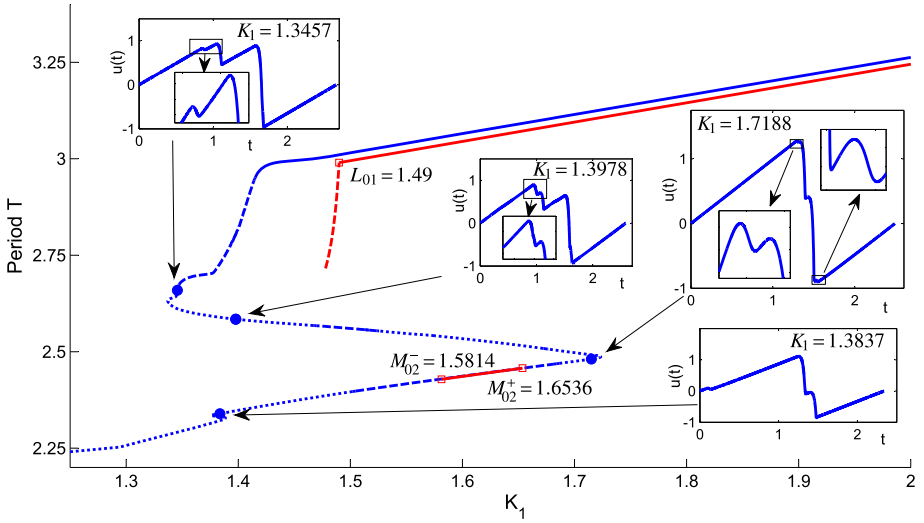

Fig. 17 Periods of $\varepsilon = 0$ singular solutions and the numerically computed $\varepsilon = 0.02$ solution branch for the same parameters as Fig. 16. *Insets* show profiles of $\varepsilon = 0.02$ trimodal and quadrimodal solutions. The solution with $K_1 = 1.3457$ is stable, the others are unstable

In Figs. 16, 17, 18 and 19 we illustrate the change in the dynamics near to $K_1 = L_{01}$ as A passes through 7; the second cusp-like bifurcation indicated by (5.1). Figures 16 and 17 demonstrate that for $\varepsilon = 0.02$ and $A = 6.98$ there is a transition from a bimodal to a

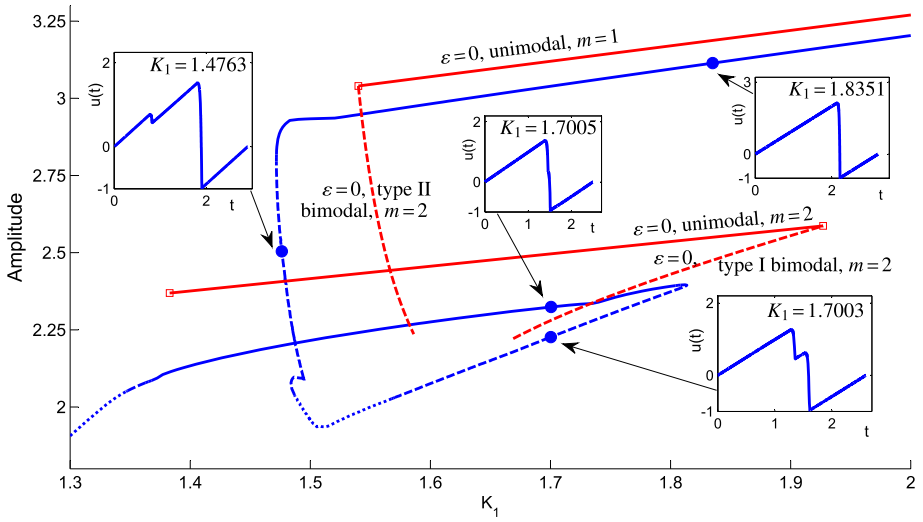

Fig. 18 Amplitudes of Type I and II bimodal singular solutions with $m = 2$ and unimodal solutions with $m = 1$ and $m = 2$ for $A = 7.08$, $K_2 = 0.5$ and $n = 0$. The numerically computed principal branch of periodic orbits with $\varepsilon = 0.02$ is also shown. *Insets* show profiles of $\varepsilon = 0.02$ periodic orbits which correspond to stable unimodal, and unstable type I and type II bimodal solutions

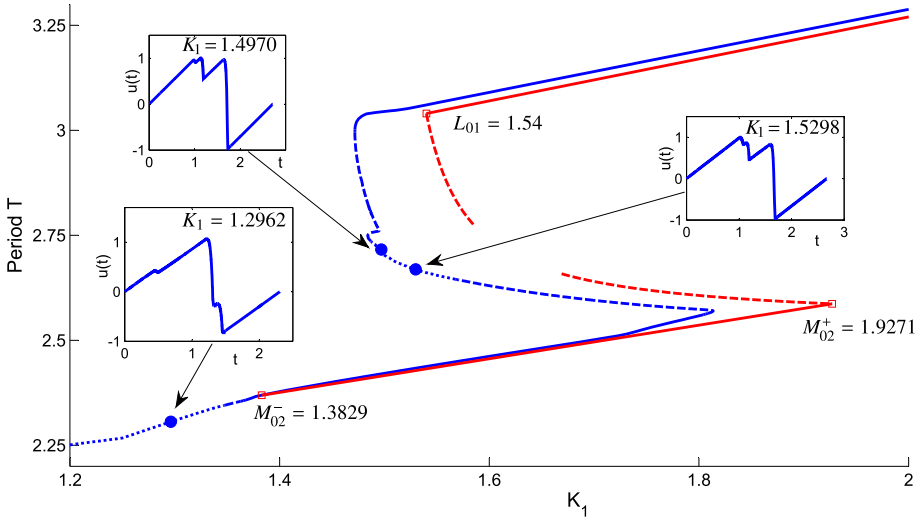

Fig. 19 Periods of $\varepsilon = 0$ singular solutions and the numerically computed $\varepsilon = 0.02$ solution branch for the same parameters as Fig. 18. *Insets* show profiles of unstable trimodal solutions on the $\varepsilon = 0.02$ branch

unimodal solution close to $K_1 = L_{01}$ without a fold bifurcation, while for $A = 7.08$ the same transition is associated with a fold bifurcation. As was the case with the first cusp-like bifurcation for $\varepsilon = 0.02$ this transition occurs for a value of K_1 slightly less than L_{01} both when $A = 6.98$ and $A = 7.08$. Also, whereas the fold appears when $A = 7$ for the singular solution with $\varepsilon = 0$, additional computations with other values of A (not shown) suggest that

for $\varepsilon = 0.02$ the fold bifurcation associated with the point $K_1 = L_{01}$ disappears at about $A = 7.04$.

Figures 18 and 19 also indicate good agreement between the singular and $\varepsilon = 0.02$ solutions near to the fold point $K_1 = M_{02}^+$, with the $\varepsilon = 0.02$ solution having a fold bifurcation associated with the solution profile transitioning from unimodal to bimodal with $K_1 \approx 1.8137$ slightly less than $M_{02}^+ = 1.9271$. The insets with $K_1 = 1.4970$ and 1.5298 in Fig. 19 for $A = 7.08$ show that trimodal solutions again occur for $\varepsilon = 0.02$ in the gap between the two intervals of bimodal solutions, just as was previously seen for $A = 4.54$ in Fig. 15.

Figures 16 and 17 show a significant difference between the dynamics near to the second cusp-like bifurcation compared to the first one. Although for $\varepsilon = 0.02$ and $A \lessapprox 7$ there is no longer a fold bifurcation near to $K_1 = L_{01}$ and there are no folds associated with transitions from unimodal to bimodal solutions, there are still fold bifurcations on the branch. Insets in Fig. 17 show trimodal solution profiles close to each of these folds. The $\varepsilon = 0$ singular solutions also show differences between the first and second cusp-like bifurcation, since when $A = 4.48$ there are type I bimodal solutions for $K_1 < L_{00}$ whereas for $A = 6.98$ there are no type I bimodal solutions, but there is a small interval of $m = 2$ unimodal solutions which coexist with the $m = 1$ unimodal solutions. Figure 17 shows that the $\varepsilon = 0.02$ branch has solutions whose K_1 values and periods almost exactly agree with those of the unimodal $m = 2$ singular solutions while the inset for $K_1 = 1.601$ in Fig. 16 shows that while the $\varepsilon = 0.02$ solution has smaller amplitude and is bimodal, its profile is close to unimodal.

The inset for $K_1 = 1.2962$ shows a trimodal solution for $\varepsilon = 0.02$ occurring before the pair of fold bifurcations. Such a solution is also seen in Fig. 15, and they seem to be ubiquitous, also arising even when the folds disappear (see inset for $K_1 = 1.5997$ in Fig. 13).

6 Other Solutions and Bifurcations

In this section we study some of the other solutions and bifurcations that can arise with (1.1). In Sects. 4 and 5 we were mainly concerned with the fold and cusp-like bifurcations predicted by Theorems 3.3 and 3.4. The folds occurred between legs of unimodal solutions, and as noted in the discussion after Theorem 3.1, we require $A > 3$ to have more than one leg of unimodal solutions on the principal $n = 0$ branch of periodic solutions. So we begin this section by considering the dynamics when $A \in (1, 3)$. Noting that Theorem 3.1 guarantees the existence of unimodal solutions for all K_1 sufficiently large *unless* $m = m^0(n) = n(A-1)$ and $A \leqslant 1 + K_2/(1 + K_2)$ we first consider this exceptional case. On the principal branch this occurs when $m = n = 0$ and taking $K_2 = 0.5$ with $A \in [1, 4/3]$. Consequently we consider the dynamics with $A = 7/6$, as shown in Fig. 20.

Verifying the conditions of Theorem 2.4 we find that there is a type II bimodal solution with $n = m = 0$ when $A = 7/6$ for all $K_1 > 0.59816$ which is shown in Fig. 20. With $\varepsilon = 0.05$, DDEBiftool finds a Hopf bifurcation at $K_1 \approx 0.5373$ leading to a branch of stable periodic solutions which exist for all larger values of K_1. Close to the Hopf bifurcation these solutions are unimodal and sinusoidal, but for all $K_1 > 1.5167$ these solutions have two local maxima per period, and closely resemble type II bimodal solutions (see $K_1 = 1.9817$ and $K_1 = 6.8797$ insets in Fig. 20). There is also very good agreement for $K_1 > 1$ between the amplitude of the $\varepsilon = 0$ singular solutions given by Theorem 2.4 and the numerically found $\varepsilon = 0.05$ solutions. Type II bimodal singular solutions and their $\varepsilon > 0$ counterparts

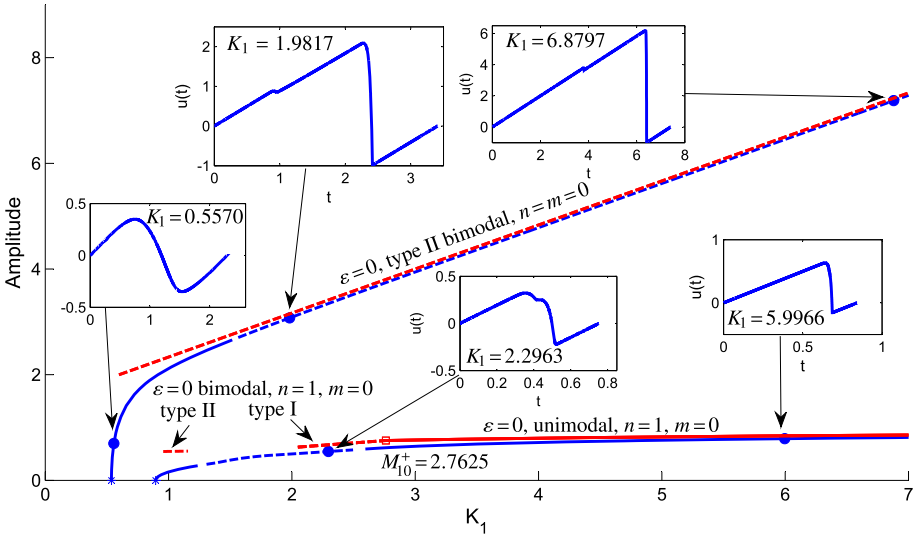

Fig. 20 The first two bifurcation branches with $A = 7/6$, $\varepsilon = 0.05$ and $\gamma = a_1 = c = 1$, $K_2 = 0.5$. Also shown are the corresponding $\varepsilon = 0$ singular solution branches, and *insets* show profiles of periodic solutions for $\varepsilon = 0.05$ at different points on the branches. The $\varepsilon = 0.05$ solutions on the first branch are all stable, and those on the second branch all unstable; DDEBiftool does not detect any secondary bifurcations

are also found for all K_1 sufficiently large for other values of $A \in (1, 1 + K_2/(1 + K_2))$ when $m = m^0(n) = n(A - 1)$.

Figure 20 also shows the $n = 1$ branch for $A = 7/6$. By Theorem 3.1(i) there is a unimodal singular solution with $n = 1$, $m = 0$ for all $K_1 > M_{10}^+ = 2.7625$, while verifying the conditions of Theorem 2.3 reveals that there is a type I bimodal solution for $K_1 \in (2.0481, M_{10}^+)$. At $K_1 = M_{10}^+$ the two solutions coincide, with $T_2 \to 0$ as $K_1 \to M_{10}^+$ for the type I bimodal solution. Theorem 3.3 deals with unimodal and type I bimodal solutions coinciding at $K_1 = M_{nm}^+$ in a fold-like bifurcation. That theorem does not apply here because we have $m = 0 < n(A - 1) = 1/6$ outside its range of validity, nevertheless we still have a transition between the two types of solutions, but here it occurs without the fold-like bifurcation. With $\varepsilon = 0.05$, DDEBiftool finds all the solutions on the corresponding branch to be unstable with a transition between bimodal and unimodal solutions close to $K_1 = M_{10}^+$.

Next we consider $A \in (4/3, 3)$ for which Theorem 3.1 guarantees the existence of a unimodal singular solution with $n = m = 0$ on the principal branch for all K_1 sufficiently large, but for which with $n = 0$ there is no value of m which satisfies the conditions of Theorem 3.3 or 3.4, and so we do not expect fold bifurcations of periodic orbits. Taking $A = 1.5$, Theorem 3.1(i) gives the existence of unimodal singular solutions with $n = m = 0$ for $K_1 > M_{00} = 5$. Similarly to the $n = 1$ branch of the previous example, verifying the conditions of Theorem 2.3 we find a type I bimodal singular solution with $n = m = 0$ for $K_1 \in (3.3508, M_{00})$. For $\varepsilon = 0.05$, using DDEBiftool we numerically compute the principal solution branch from the Hopf bifurcation (at $K_1 \approx 0.7363$), finding stable bimodal periodic solutions for $K_1 \in (3.3414, 5.0543)$, and stable unimodal solutions for $K_1 > 5.0543$ as shown in Fig. 21. The parameter ranges and amplitudes of the solutions with $\varepsilon = 0.05$ are seen to be very close to the $\varepsilon = 0$ singular solutions. Solutions are also stable on the initial part of the branch and unimodal for $K_1 \in (0.7363, 0.8586)$ and bimodal for

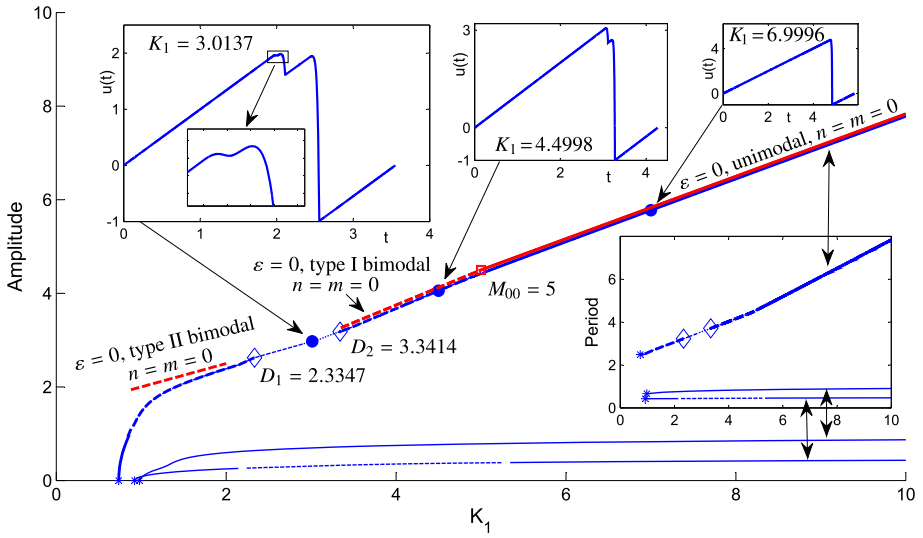

Fig. 21 Amplitude and period plots for the first three branches of periodic solutions with *insets* showing unimodal, bimodal and trimodal solutions on the prinicpal branch for $A = a_2 = 1.5$, $\varepsilon = 0.05$ and $\gamma = a_1 = c = 1$, $K_2 = 0.5$. DDEBiftool detects period doubling bifurcations at $K_1 = D_1$ and D_2, and the solutions on the principal branch are stable except for K_1 between these values. Also shown are the unimodal and type I bimodal singular solutions corresponding to the principal branch

$K_1 \in (0.8586, 2.3347)$. However, the solutions on the principal branch are unstable in the range $K_1 \in (D_1, D_2) = (2.3347, 3.3414)$ with DDEBiftool detecting period doubling bifurcations (characterized by a real Floquet multiplier passing through -1) at both ends of this interval. On the principal branch trimodal solutions are found for $K_1 \in (2.9016, 3.3112)$ while the solutions are bimodal in the rest of the interval (D_1, D_2).

In Fig. 22 we show the resulting branch of $\varepsilon = 0.05$ stable period-doubled solutions for $K_1 \in (D_1, D_2)$. The branch is computed from $K_1 = D_1$ and appears to terminate at $K_1 = D_2$, though numerical computation of the branch is very difficult near to $K_1 = D_2$. *Insets* show profiles of the resulting stable periodic solutions which all have period close to 7 and mainly have four local maxima per period, except for $K_1 \in (2.5247, 2.6909)$ where the first peak splits into two (reminiscent of the transitions from bimodal to trimodal solutions seen in Sect. 4) resulting in periodic solutions with five local maxima per period.

We do not have a characterization from the singular solutions of when to expect period doubling bifurcations. To determine the parameter ranges where period doubled orbits can occur we could parameterise the period doubled singular periodic orbits. This would be similar to a perturbation of two copies of the parameterisations illustrated in Figs. 3 and 4 and would involve twenty parametrisation intervals and more algebraic manipulation than we care to contemplate. We note that at the end of the interval of validity of the type I bimodal solution at $K_1 = 3.3508$ the left inequality in (2.21) is tight, and fails for smaller values of K_1. This is the same inequality that failed at the transition between type I bimodal and trimodal solutions between the fold bifurcations at $K_1 = L_{nm-1}$ and $K_1 = M^+_{nm}$ which we studied in Sect. 4. Given the proximity of the end of the interval of type I bimodal singular solution at $K_1 = 3.3508$ to the period doubling bifurcation with $\varepsilon = 0.05$ at $K_1 = 3.3414$ and the transition from bimodal to trimodal solutions at $K_1 = 3.3112$ we suspect that in the limit as $\varepsilon \to 0$ the singular solutions undergo a period doubling bifurcation at the same

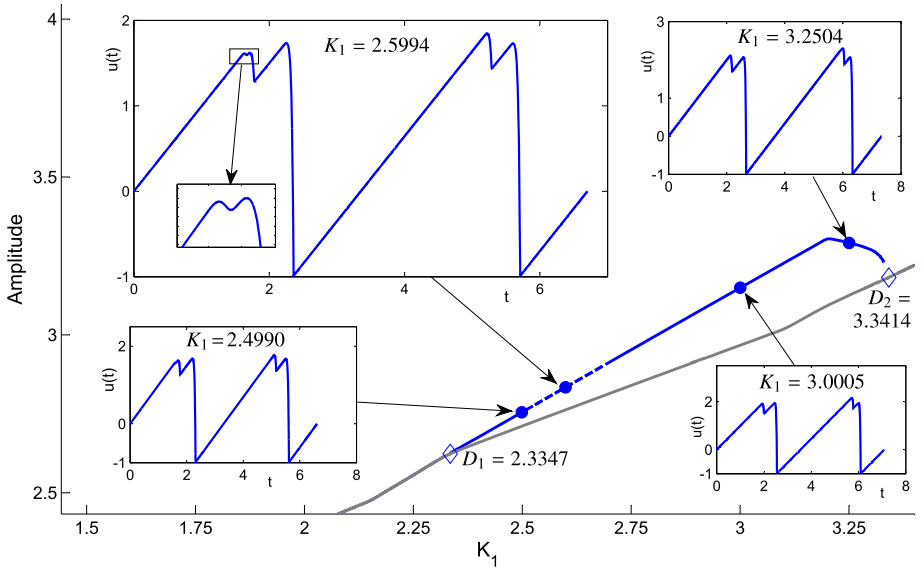

Fig. 22 Branch of stable period doubled solutions for $K_1 \in (D_1, D_2)$ with *insets* showing solution profiles. The parameters are the same as in Fig. 21, and the principal branch of periodic solutions from Fig. 21 is redrawn in *gray* here

parameter value where the periodic solution transitions from type I bimodal to trimodal. The behaviour seen in this example contrasts with the examples in Sects. 4 and 5 where no period doubling bifurcations were detected between the fold bifurcations.

We have already seen examples corresponding to Theorem 3.4(i) and (ii) with unimodal and type II bimodal solutions which coincide at $K_1 = L_{nm-1}$ with or without a fold bifurcation. Figure 23 illustrates Theorem 3.4(iii), showing a type II bimodal singular solution which exists for $K_1 < L_{nm-1}$ and a unimodal solution for $K_1 > M^-_{nm-1}$, where $M^-_{nm-1} > 1 > L_{nm-1}$. When $n = 0$ we have $L_{nm^*} = 1$ at $A = 1 + m(2 + K_2)$ so $A = 3 + K_2, 5 + 2K_2, 7 + 3K_2, \ldots$ and so separated unimodal and type II bimodal solutions will occur for A slightly smaller than these values. In Fig. 23 we consider $K_2 = 0.5$ and $A = 5.75 < 6 = 5 + 2K_2$.

Theorems 2.2 and 2.3 require $K_1 > 1$ for unimodal and type I bimodal solutions to exist, but Theorem 2.4 only requires $K_1 > 1 - K_2$ for the construction type II bimodal solutions, and Fig. 23 shows an example of type II bimodal solutions which exist for $K_1 < 1$. Figure 23 also shows a numerically computed branch of periodic orbits with $\varepsilon = 0.005$ which passes very close to the legs of bimodal type I and unimodal singular solutions. While the type II bimodal solutions exist for $K_1 \in (0.6621, 0.875)$ the $\varepsilon = 0.005$ branch has bimodal solutions for $K_1 \in (0.6444, 0.7822)$ with the inset solution profile for $K_1 = 0.7522$ showing that these resemble type II singular solutions. The $\varepsilon = 0.005$ branch also has unimodal solutions for $K_1 > 1.0126$ which approximate the unimodal singular solutions existing for $K_1 > 1.0348$. It was found that the period of the solutions on the $\varepsilon = 0.005$ branch increases monotonically from $T \approx 2.2478$ at the Hopf bifurcation and crosses $T = 2.375$ at $K_1 \approx 0.84265$. At this value of K_1 the period T satisfies $2T = 4.75 = a_2 - a_1$, that is the difference between the delays is exactly two periods. For the singular solutions $2T = a_2 - a_1$ when $K_1 = L_{01} = 0.875$ at the end of the interval of bimodal type II solutions. Figure 23 suggests that there is not a bifurcation near to $K_1 = L_{nm-1} < 1$

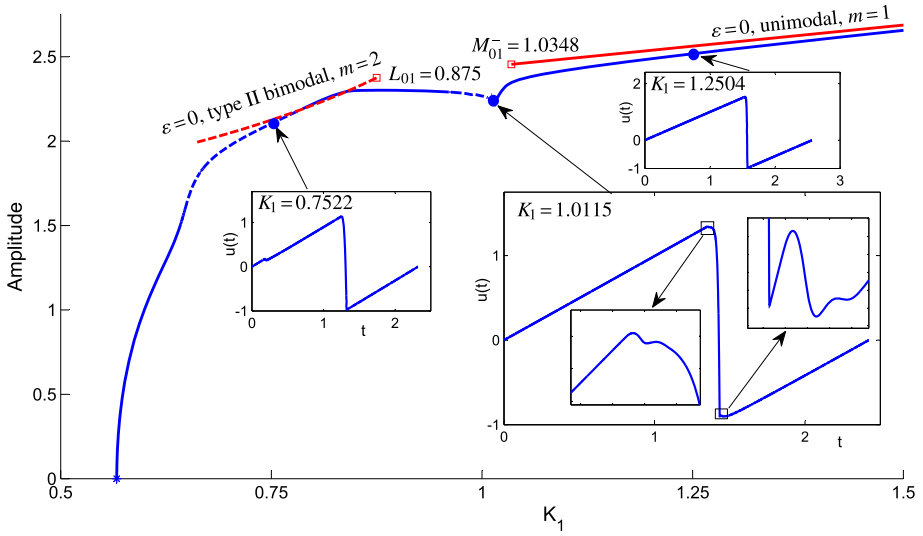

Fig. 23 Amplitude plot of type II bimodal solution with $n = 0$ and $m = 2$ which exists for $K_1 < L_{01} < 1$ and a unimodal singular solution with $n = 0$ and $m = 1$ which exists for $K_1 > M_{01}^- > 1$. Here $A = a_2 = 5.75$ and as before $K_2 = 0.5$, $a_1 = 1$ and $c = 1$. Also shown is the corresponding branch of periodic orbits with $\varepsilon = 0.005$ computed using DDEBiftool. This branch bifurcates from the steady state solution at $K_1 \approx 0.5665$. *Insets* show examples of $\varepsilon = 0.005$ stable solutions for $K_1 < L_{01}$ and $K_1 > M_{01}^-$ and an unstable solution for $K_1 = 1.0115 \in (L_{01}, M_{01}^-)$

when the conditions of Theorem 3.4(iii) are satisfied, but neither do the solutions transition directly from type II bimodal to unimodal solutions, as occurs in Theorem 3.4(i) and (ii). We do not have an explanation for the dynamics for $K_1 \in (L_{01}, M_{01}^-)$ in Fig. 23, but note with $\varepsilon = 0.005$ bimodal solutions are seen for $K_1 \in (0.9606, 1.0066)$ and multimodal solutions for $K_1 \in (1.0066, 1.0126)$, and the solution appears to transition directly from multimodal to unimodal at the kink in the bifurcation branch with $K_1 = 1.0126$.

Another example where bimodal type II singular solutions could exist for $K_1 < 1$ was already seen in Fig. 10. Figure 10 illustrated the boundary between Theorem 3.4(ii) and (iii) with $m = m^*(n)$ and $L_{nm} = M_{nm}^- = 1$.

Thus far, we have concentrated our attention on unimodal and bimodal solutions, but noted that trimodal and quadrimodal solutions arise between legs of type I and II bimodal solutions. Figure 24 shows examples of multimodal solutions with up to seven local minima per period (see the $K_1 = 1.372$ inset) for $\varepsilon = 0.02$. The parameters in Fig. 24 are the same as those considered in Figs. 12 and 13, where we studied the cusp-like bifurcation at $K_1 = L_{00} = 2$ with $A = 4.5$. Figure 24 shows that even for $A < 4.5$ when there are no fold bifurcations near to $K_1 = L_{00}$, there are still six fold bifurcations earlier on the principal branch, and there are solutions with multimodal profiles near to each of these folds. The multimodal solution profiles shown in the figure for $K_1 \in (1.3, 1.44)$ all have well-defined 'sawteeth' with the periodic solution profile having gradient close to $1/c = 1$ before each local maxima and large negative gradient afterwards. It seems plausible that the fold bifurcations associated with the transitions between unimodal and bimodal solution profiles that we studied earlier are just the simplest example of a sequence of such bifurcations that occur at points where the number of local maxima in the periodic solution profile changes. In principle, Definition 1.1 and our techniques could be used to locate such bifurcations in the $\varepsilon \to 0$ limit.

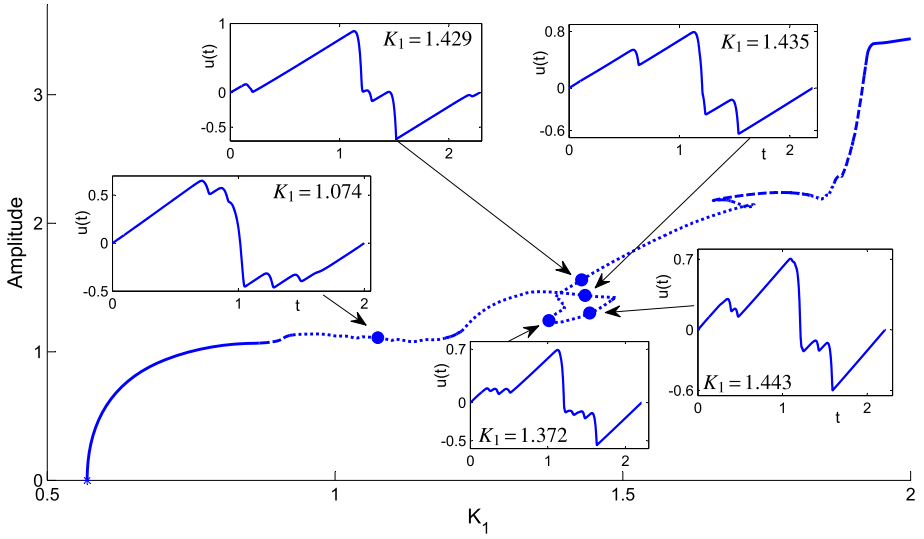

Fig. 24 Amplitude plot of principal branch of periodic solutions with $\varepsilon = 0.02$, $A = a_2 = 4.48$, $a_1 = c_1 = 1$ with *insets* showing profiles of unstable multimodal solutions that occur on the branch. Recall that *dotted lines* indicate multimodal solutions, *dashed* indicate bimodal and *solid lines* show unimodal solutions

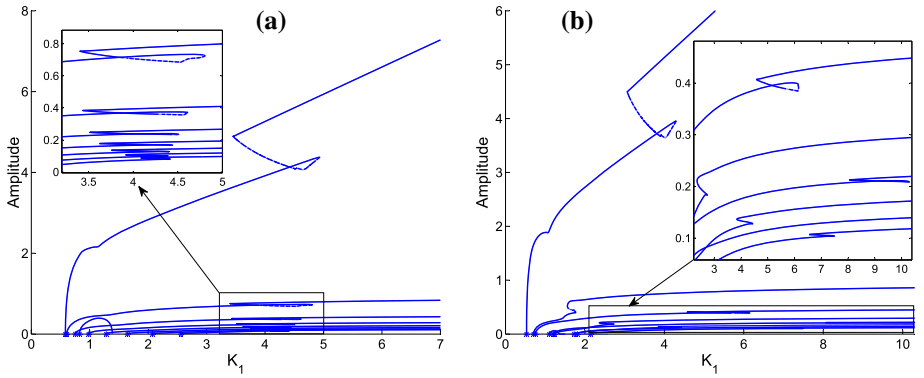

Fig. 25 Amplitudes of several branches of periodic solutions with $\varepsilon = 0.05$, $K_2 = 0.5$, $a_1 = c = 1$ and **a** $A = 6$ and **b** $A = (9 + \sqrt{5})/2$

We have mainly considered the principal branch of periodic solutions corresponding to singular solutions with $n = 0$, since this is the branch on which stable solutions can be observed, but it was demonstrated in [19] that there are infinitely many Hopf bifurcations for $\varepsilon > 0$ and we finish this work by considering the alignment of the bifurcations on the different branches. This is illustrated in Figs. 25 and 26 for $\varepsilon = 0.05$. With $A = 6$ we saw earlier that in the limit as $\varepsilon \to 0$ the fold bifurcations occur on the principal $n = 0$ branch at $K_1 = L_{00} = 3.5$ and $K_1 = M_{01}^{+} = 5$. Figure 25a suggests that the folds on the other (unstable) branches of periodic solutions all occur between the same K_1 values. Contrast this with Fig. 26 where with $A = 5.5$ there seems to be an alignment between the bifurcations on every second branch, and Fig. 25(b) where with A equal to 4 plus the golden ratio there does not appear to be any alignment between the bifurcations on different branches.

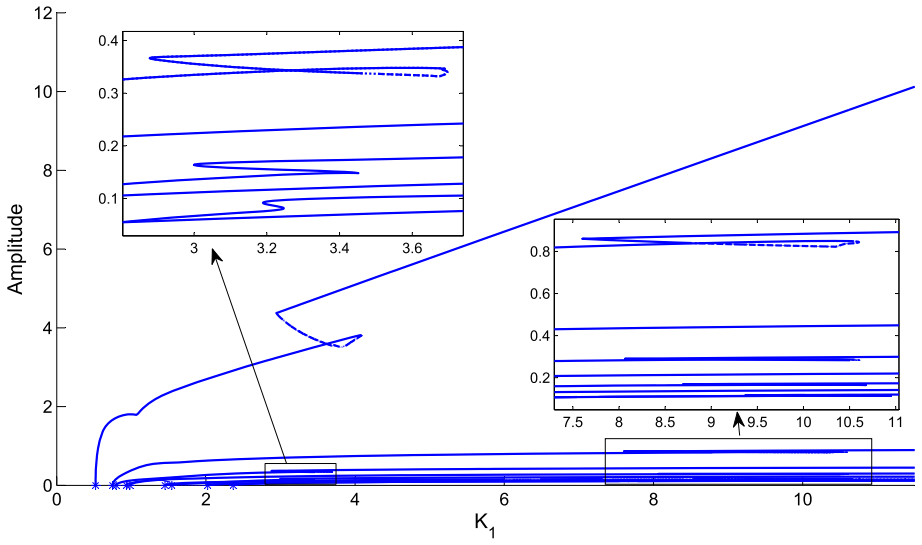

Fig. 26 Amplitudes of several branches of periodic solutions with $\varepsilon = 0.05$, $K_2 = 0.5$, $a_1 = c = 1$ and $A = 5.5$

To explain this alignment notice that in the singular limit $\varepsilon \to 0$ by Theorems 3.3 and 3.4(i) for suitable integer value(s) of m there are fold bifurcations on the nth branch at $K_1 = L_{nm}$ and $K_1 = M^+_{nm-1}$. But L_{nm} defined by (3.3) and M^+_{nm} defined as the larger zero of $G_{nm}(K_1)$ (see (2.15)) both depend on n and m only through the common term $m - n(A-1)$. Hence if $A = p/q$ is rational then defining

$$n_k = n_0 + kq, \quad m_k = m_0 + k(p-q), \quad k \in \mathbb{N}$$

we see that

$$m_k - n_k(A-1) = m_0 - n_0(A-1),$$

and hence $L_{n_k m_k} = L_{n_0 m_0}$ and $M^+_{n_k m_k} = M^+_{n_0 m_0}$ for each integer k and for each $n_0 = 0, 1, 2, \ldots, q-1$. Hence these singular fold bifurcations align on every q-th branch when $A = p/q$ is rational. Thus, when A is integer these bifurcations align on all the branches (eg $A = 6$, see Fig. 25a), when $A = p/2$ the bifurcations align on every second branch (eg $A = 5.5$, see Fig. 26), and when A is irrational there is no alignment between the bifurcations (see Fig. 25b).

Moving to the $\varepsilon > 0$ case, we see from the figures with $\varepsilon = 0.05$ that the fold bifurcations which should align exactly in the limit as $\varepsilon = 0$, actually appear to occur within shrinking subintervals of $[L_{n_0 m_0}, M^+_{n_0 m_0 - 1}]$ as n_k is increased, and for sufficiently large n_k the fold bifurcations disappear entirely. Although for each fixed n_k the folds occur for all ε sufficiently small and converge to $K_1 = L_{n_0 m_0}$ and $K_2 = M^+_{n_0 m_0 - 1}$ as $\varepsilon \to 0$ the convergence is clearly not uniform, with smaller values of ε required to create the fold bifurcations for larger values of n_k. This is not surprising, since the larger the value of n_k the smaller the period and amplitude of the $\varepsilon = 0$ singular solutions defined by Theorems 2.2, 2.3 and 2.4. But, when solving with $\varepsilon > 0$ the smaller amplitude solutions appear smoother and more sinusoidal than the larger amplitude solutions and the fold bifurcations do not occur unless ε is reduced sufficiently to resolve the sawteeth in the solution.

7 Conclusions

Through Definitions 1.1 and 1.2 we have introduced a new definition of singular solution via a double parametrisation which allows us to define a continuous parametrisation even when the limiting profile is not continuous. This reduces the problem of constructing singular solutions to a purely algebraic problem. For the DDE (1.1) with two state-dependent delays we constructed three different solution profiles in Sect. 2 and in Theorems 2.2, 2.3 and 2.4 identified parameter constraints for these unimodal and type I and type II bimodal singular solutions to exist. In Sect. 3 we investigated the parameter constraints for the singular solutions constructed in Sect. 2, and treating K_1 as a bifurcation parameter in Theorem 3.1 identified intervals of K_1 for which unimodal singular solutions exist. Theorem 3.3 identifies intervals on which type I bimodal solutions exist, and also a singular fold bifurcation where the solution profile also transitions between unimodal and type I bimodal. Theorem 3.4 identifies intervals on which type II bimodal solutions exist, and a point where the solution profile transitions between unimodal and type II bimodal, with or without a singular fold bifurcation, and we hence identify a singular codimension-two bifurcation.

The results in Sects. 2 and 3 all follow from our definition of singular solution following purely algebraic arguments. Although we do not prove analytically that the singularly perturbed DDE (1.1) has corresponding periodic solutions for $0 < \varepsilon \ll 1$, in Sect. 4 we demonstrate numerically using DDEBiftool that the singular periodic solutions that we found do persist for $\varepsilon > 0$. Moreover, we find that there is very good agreement between the parts of the bifurcation diagram determined by the unimodal and bimodal singular solutions, and the numerically computed small ε branches and profiles. The $\varepsilon > 0$ computations also reveal intervals of bistability of unimodal periodic solutions and unstable solutions with two, three and more local maxima per period.

In Sect. 4 we saw that for $0 < \varepsilon \ll 1$ fold bifurcations occur close to $K_1 = L_{nm}$ and $K_1 = M^+_{nm}$. In Sect. 5, we considered the codimension-two bifurcations predicted by Theorem 3.4 where the fold at $K_1 = L_{nm}$ vanishes and for $0 < \varepsilon \ll 1$ found the predicted cusp bifurcations, and associated stable bimodal periodic orbits (see Figs. 12, 16)

In Sect. 6, Theorem 3.1(i) led us to find stable periodic orbits with two local maxima per period when $\varepsilon > 0$ (Fig. 20). A period doubling bifurcation also gives rise to stable periodic orbits with up to 5 local maxima per period (see Fig. 22). We were also able to use our singular solution theory to predict the alignment of the fold bifurcations on different solution branches.

In addition to the fold bifurcations associated with the transition between unimodal and bimodal solutions predicted by Theorems 3.3 and 3.4 we also found many examples of solutions of (1.1) with three or more local maxima per period sometimes with fold bifurcations associated to the transitions between such solutions. In contrast the one delay DDE (1.3) has only been seen to have periodic orbits with one local maxima per period, and no secondary bifurcations on the branches of periodic orbits [19].

In conclusion, the state-dependent DDE (1.1) has very rich and interesting dynamics in the $\varepsilon \to 0$ singular limit, and the concept of singular solution that we introduce in Definitions 1.1 and 1.2 is a useful tool in the study of those dynamics. While we have not proved rigourously that the singular solutions that we construct persist for $\varepsilon > 0$, we have shown numerically that they do, and identified where bifurcations occur. A useful first step in proving convergence as $\varepsilon \to 0$ is to identify what the singularly perturbed solutions should converge to. With this work that first step is resolved.

Acknowledgments Tony Humphries thanks John Mallet-Paret and Roger Nussbaum for introducing him to this problem and patiently explaining their results in the one delay case. He is also grateful to NSERC (Canada) for funding through the Discovery Grants program. Renato Calleja thanks the Department of Mathematics and Statistics at McGill for their hospitality during his time as a postdoctoral fellow and on several return visits to Montreal. He is also grateful to NSERC and the Centre de recherches mathématiques, Montréal for funding and to FQRNT, Québec for a PBEEE award. Daniel Bernucci and Michael Snarski are grateful to NSERC for Undergraduate Student Research Awards. Namdar Homayounfar thanks the Institut des Sciences Mathématiques, Montréal for an Undergraduate Summer Scholarship.

References

1. Bellen, A., Zennaro, M.: Numerical methods for delay differential equations. OUP, Oxford (2003)
2. Bellen, A., Maset, S., Zennaro, M., Guglielmi, N.: Recent trends in the numerical solution of retarded functional differential equations. Acta Numer. **18**, 1–110 (2009)
3. Broer, H.W., Kaper, T.J., Krupa, M.: Geometric desingularization of a cusp singularity in slow-fast systems with applications to Zeeman's examples. J. Dyn. Differ. Equ. **25**, 925–958 (2013)
4. Calleja, R.C., Humphries, A.R., Krauskopf, B.: Resonance phenomena in a scalar delay differential equation with two state-dependent delays (2015) (in preparation)
5. Chiba, H.: Periodic orbits and chaos in fast-slow systems with Bogdanov-Takens type fold points. J. Differ. Equ. **250**, 112–160 (2011)
6. Chow, S.-N., Lin, X.-B., Mallet-Paret, J.: Transition layers for singularly perturbed delay differential equations with monotone nonlinearities. J. Dyn. Differ. Equ. **1**, 3–43 (1989)
7. De Luca, J., Humphries, A.R., Rodrigues, S.B.: Finite element boundary value integration of Wheeler-Feynman electrodynamics. J. Comput. Appl. Math. **236**, 3319–3337 (2012)
8. Desroches, M., Guckenheimer, J., Krauskopf, B., Kuehn, C., Osinga, H., Hinke, Wechselberger, M.: Mixed-mode oscillations with multiple time scales. SIAM Rev. **54**, 211–288 (2012)
9. Diekmann, O., van Gils, S.A., Verduyn Lunel, S.M., Walther, H.-O.: Delay Equations: Functional-, Complex-, and Nonlinear Analysis. Springer, Berlin (1995)
10. Eichmann, M.: A local Hopf bifurcation theorem for differential equations with state-dependent delays. PhD thesis, Universität Gießen, Germany (2006)
11. Engelborghs, K., Luzyanina, T., Roose, D.: Numerical bifurcation analysis of delay differential equations using DDE-Biftool. ACM Trans. Math. Soft. **28**, 1–21 (2002)
12. Erneux, T.: Applied Delay Differential Equations. Springer, New York (2009)
13. Foley, C., Mackey, M.C.: Dynamic hematological disease: a review. J. Math. Biol. **58**, 285–322 (2009)
14. Guglielmi, N., Hairer, E.: Asymptotic expansions for regularized state-dependent neutral delay equations. SIAM J. Math. Anal. **44**, 2428–2458 (2012)
15. Guo, S., Wu, J.: Bifurcation Theory of Functional Differential Equations. Applied Mathematical Sciences, vol. 184. Springer, New York (2013)
16. Hale, J., Verduyn Lunel, S.M.: Introduction to Functional Differential Equations. Springer, New York (1993)
17. Hartung, F., Krisztin, T., Walther, H.-O., Wu, J.: Functional differential equations with state-dependent delays: theory and applications. In: Cañada, A., Drábek, P., Fonda, A. (eds.) Handbook of Differential Equations: Ordinary Differential Equations, vol. 3, pp. 435–545. Elsevier/North-Holland, Amsterdam (2006)
18. Hu, Q., Wu, J.: Global Hopf bifurcation for differential equations with state-dependent delay. J. Differ. Equ. **248**, 2801–2840 (2010)
19. Humphries, A.R., DeMasi, O.A., Magpantay, F.M.G., Upham, F.: Dynamics of a delay differential equation with multiple state-dependent delays. Disc. Cont. Dyn. Syst. A **32**, 2701–2727 (2012)
20. Insperger, T., Stépán, G., Turi, J.: State-dependent delay in regenerative turning processes. Nonlinear Dyn. **47**, 275–283 (2007)
21. Ivanov, A.F., Sharkovsky, A.N.: Oscillations in singularly perturbed delay equations. In: Jones, C.K.R.T., Kirchgraber, U., Walther, H.O. (eds.) Dynamics Reported, Expositions in Dynamical Systems, vol. 1, pp. 164–224. Springer, New York (1992)
22. Kozyreff, G., Erneux, T.: Singular Hopf bifurcation in a differential equation with large state-dependent delay. Proc. R. Soc. A **470**, 2162 (2014)
23. Liz, E., Rost, G.: Global dynamics in a commodity market model. J. Math. Anal. Appl. **398**, 707–714 (2013)

24. Mackey, M.C.: Commodity price fluctuations: price dependent delays and nonlinearities as explanatory factors. J. Econ. Theory **48**, 497–509 (1989)
25. Magalhaẽs, L.T.: The asymptotics of singularly perturbed functional differential equations: distributed and concentrated delays are different. J. Math. Anal. Appl. **105**, 250–257 (1985)
26. Mallet-Paret, J., Nussbaum, R.D.: Global continuation and asymptotic behavior for periodic solutions of a differential-delay equation. Ann. Mat. Pura. Appl. **145**, 33–128 (1986)
27. Mallet-Paret, J., Nussbaum, R.D.: Boundary layer phenomena for differential-delay equations with state-dependent time lags, I. Arch. Ration. Mech. Anal. **120**, 99–146 (1992)
28. Mallet-Paret, J., Nussbaum, R.D., Paraskevopoulos, P.: Periodic solutions for functional differential equations with multiple state-dependent time lags. Top. Methods Nonlinear Anal. **3**, 101–162 (1994)
29. Mallet-Paret, J., Nussbaum, R.D.: Boundary layer phenomena for differential-delay equations with state-dependent time lags: II. J. Reine Angew. Math. **477**, 129–197 (1996)
30. Mallet-Paret, J., Nussbaum, R.D.: Boundary layer phenomena for differential-delay equations with state-dependent time lags: III. J. Differ. Equ. **189**, 640–692 (2003)
31. Mallet-Paret, J., Nussbaum, R.D.: Superstability and rigorous asymptotics in singularly perturbed state-dependent delay-differential equations. J. Differ. Equ. **250**, 4037–4084 (2011)
32. Mallet-Paret, J., Nussbaum, R.D.: Periodic solutions of differential equations with two state-dependent delays (2015) (in preparation)
33. MATLAB R2014b, The MathWorks Inc., Natick, MA, USA (2014)
34. Pellegrin, X., Grotta-Ragazzo, C., Malta, C.P., Pakdaman, K.: Metastable periodic patterns in singularly perturbed state-dependent delayed equations. Physica D **271**, 48–63 (2014)
35. Sharkovsky, A.N., Maistrenko, YuL, Romanenko, EYu.: Difference Equations and their Applications. Kluwer, Dordrecht (1993)
36. Sieber, J.: Dimension reduction for periodic boundary value problems of functional differential equations. Disc. Cont. Dyn. Syst. A **32**, 2607–2651 (2012)
37. Smith, H.: An Introduction to Delay Differential Equations with Applications to the Life Sciences. Springer, New York (2010)
38. Walther, H.-O.: On a model for soft landing with state dependent delay. J. Dyn. Differ. Equ. **19**, 593–622 (2003)